Meteorology, not emissions, helps explain an upward trend in atmospheric methane across the US

Feng Leyang[1], Tavakkoli Sakineh[1], Jordaan Sarah[1], Andrews Arlyn Elizabeth[2], Benmergui Joshua[3], Waugh Darryn W.[1], Zhang Mingyang[1], Gaeta Dylan C.[1], and Miller Scot[1]

[1]Johns Hopkins University
[2]National Oceanic and Atmospheric Administration (NOAA)
[3]Harvard University

November 16, 2022

Abstract

US natural gas production increased by ˜43% between 2005 and 2015, but there is disagreement in the scientific literature on whether this growth led to increased methane emissions. In this study, we evaluate the possible contributions of emissions versus meteorology to an upward trend in US atmospheric methane observations during 2007-2015. We find that interannual variability (IAV) in meteorology yields an apparent upward trend in atmospheric methane across much of the US. We further find that IAV in atmospheric methane at several observation sites is correlated with IAV in local wind speed. Overall, our results show that US trends in atmospheric methane largely reflect variability in meteorology, and are unlikely to be a direct reflection of trends in emissions. The results of this study therefore lend support for the conclusion that there was little upward trend in US methane emissions during this time.

Meteorology, not emissions, helps explain an upward trend in atmospheric methane across the US

Leyang Feng[1], Sakineh Tavakkoli[2], Sarah M. Jordaan[2], Arlyn E. Andrews[3], Joshua S. Benmergui[4], Darryn W. Waugh[5], Mingyang Zhang[1], Dylan C. Gaeta[1] and Scot M. Miller[1]

[1]Department of Environmental Health and Engineering, Johns Hopkins University, Baltimore, MD

[2]School of Advanced International Studies, Johns Hopkins University, Washington, DC

[3]Global Monitoring Laboratory, Earth System Research Laboratories, NOAA, Boulder, CO

[4]John A. Paulson School of Engineering and Applied Sciences, Harvard University, Boston, MA

[5]Department of Earth & Planetary Sciences, Johns Hopkins University, Baltimore, MD

Corresponding author: Leyang Feng (lfeng13@jhu.edu)

Key Points:

- Meteorology helps explain an upward trend in observed atmospheric methane concentrations in the United States between years 2007 and 2015.
- Trends in local meteorological processes (e.g., annually-averaged horizontal wind speed) correlate with atmospheric methane trends at many locations.
- This work supports for the conclusion that there was little or no trend in US methane emissions during this time.

Abstract

US natural gas production increased by ~43% between 2005 and 2015, but there is disagreement in the scientific literature on whether this growth led to increased methane emissions. In this study, we evaluate the possible contributions of emissions versus meteorology to an upward trend in US atmospheric methane observations during 2007-2015. We find that interannual variability (IAV) in meteorology yields an apparent upward trend in atmospheric methane across much of the US. We further find that IAV in atmospheric methane at several observation sites is correlated with IAV in local wind speed. Overall, our results show that US trends in atmospheric methane largely reflect variability in meteorology, and are unlikely to be a direct reflection of trends in emissions. The results of this study therefore lend support for the conclusion that there was little upward trend in US methane emissions during this time.

Plain Language Summary

US natural gas production increased from 18 to 27.1 trillion cubic feet per year between 2005 and 2015 as a result of the shale gas boom and the associated technological breakthrough of combining horizontal drilling and hydraulic fracturing. This increase in natural gas activity has caused concern about methane emissions, since methane is the primary constituent of natural gas and an important greenhouse gas. However, estimates of trends in US methane emissions have been ambiguous and controversial, and existing studies have reached conflicting conclusions. Furthermore, atmospheric methane levels at many US observation locations have increased faster than the global mean, raising questions about whether increasing US natural gas production has led to increased emissions. In this study, we explore the roles of changing emissions versus changing meteorology in explaining recent increases in atmospheric methane levels across the US. And we find that changing meteorology can explain this recent atmospheric methane increase. The results of this study elucidate the complex relationships between emissions and atmospheric observations and shed light on recent changes in US methane emissions.

1 Introduction

The US is one of the largest anthropogenic emitters of methane, behind only China and India (Saunois et al. 2020). Numerous recent studies indicate that US methane emissions are 48% - 76% higher than estimated by the EPA Inventory of US Greenhouse Gas Emissions and Sinks (GHGI) (Alvarez et al. 2018; Barkley et al. 2019, 2021; Caulton et al. 2019; Robertson et al. 2020; Zavala-Araiza et al. 2015). One reason for this discrepancy is that methane emissions are challenging to quantify. For example, recent studies indicate that 5% of oil and gas facilities account for over 50% of emissions (Brandt et al. 2016; see also Omara et al. 2018; Rella et al. 2015; Zavala-Araiza et al. 2015, 2017). These facilities can be difficult to find, effectively monitor, and subsequently account for in an emissions inventory that is based upon a limited number of emissions factors.

In addition, a marked increase in natural gas activity over the past 15 years has caused concern over possible increases in US methane emissions. US natural gas production increased by 43% between years 2005 and 2015, and this increase is coincident with the deployment of hydraulic fracturing and horizontal drilling technologies (US EIA, 2016). Several studies argue that increased natural gas production activity likely means increased fugitive methane emissions (Howarth et al. 2019). By contrast, EPA's GHGI indicates that total US anthropogenic methane emissions decreased by 5.0% between years 2005 - 2015 and that emissions from the natural gas sector decreased by 8.8% (US EPA, 2021). EPA attributes most of this change in natural gas emissions to decreasing exploration and distribution emissions and reports decreasing emissions factors across many areas of the natural gas sector (US EPA, 2021). These decreasing emissions factors explain why the trend in EPA's emissions inventory is opposite the trend in natural gas production.

In addition to the EPA inventory, a handful of studies based on atmospheric observations estimate trends in US methane emissions. However, these studies do not agree on whether US methane emissions increased. Turner et al. (2016) examine trends in atmospheric observations from a site in Oklahoma and from the Greenhouse Gases Observing Satellite (GOSAT). They estimate that US emissions increased by 2.5 - 4.7% per annum between years 2010 and 2014, depending on the observations analyzed. Sheng et al. (2018), also using GOSAT, report a similar upward emissions trend of 2.5±1.4% per annum between years 2010-2016. By contrast, a handful of additional studies find a much smaller increase or no increase at all. For example, Lan et al. (2019) report a trend in US emissions of 0.7±0.3% per annum (2006-2015) using in situ observation sites, Maasakkers et al. (2021) estimate a trend of 0.4% per annum (2010-2015) using observations from GOSAT, and Lu et al. (2021) estimate a trend of 0.1±0.2% per annum (2010-2017) using both GOSAT and in situ observation sites.

The purpose of this work is to help reconcile the disparate trends reported by recent studies that use atmospheric methane observations. Specifically, we hypothesize that meteorology produced an upward trend in atmospheric methane across the United States between years 2007-2015, and that this upward trend in meteorology can help explain the disagreement among existing atmospheric estimates of methane emissions trends. To answer this hypothesis, we develop meteorology and emissions trend scenarios to evaluate the plausible impacts of meteorology versus emissions on trends in atmospheric methane levels. In subsequent analyses, we further examine the correlations between inter-annual variability (IAV) in our modeled methane scenarios and IAV in specific meteorological parameters. This analysis sheds light on the specific meteorological processes that correlate with atmospheric methane trends.

2 Data and methods

2.1 Atmospheric modeling

We model atmospheric methane mixing ratios (MMR) between years 2007 and 2015 at 8 tower measurement sites in the continental US that are part of the National Oceanic and Atmospheric (NOAA) Global Monitoring Laboratory (GML) Cooperative Air Sampling Network (Andrews et al, 2014). Tall tower observations in the US greatly expanded in 2007, and the 8 tower sites included in this study have observations available during all years of the study period. We further model MMR at 80,914 GOSAT sounding locations across the continental US (CONUS) between years 2009 and 2015. GOSAT sounding locations are specifically taken from the UoL Proxy XCH_4 Retrieval Version 9 (Parker et al. 2020). This data product provides total column averaged atmospheric methane mixing ratios at GOSAT sounding locations and is used in several recent studies of methane emissions (Maasakkers et al. 2021; Sheng et al. 2018).

We model atmospheric MMR at these locations using simulations from the Stochastic Time-Inverted Lagrangian Transport model (STILT) (e.g., Lin et al. 2003). The simulations used here were generated as part of the NOAA CarbonTracker-Lagrange project (e.g., Hu et al. 2019).

STILT is a particle trajectory model; it tracks a large set of tracer particles (500 in this study), and the dispersion of those particles in the atmosphere is used to generate an influence footprint (in the units of atmospheric mixing ratio per unit of emissions). As a result of this setup, we model methane at each location and time by multiplying an individual footprint by a methane emission estimate (described below). Note that the STILT particles are driven by meteorology from the Weather Research and Forecast (WRF) model (Skamarock et al. 2008). To date, WRF-STILT has been used for atmospheric transport in numerous existing regional methane and greenhouse gas modeling studies (Hu et al. 2019; Miller et al. 2013, 2014, 2015; Nehrkorn et al. 2010). The WRF simulations have a nested spatial resolution of 10 km over CONUS and 40 km over remaining regions of North America. The STILT footprints are run for a total of 10 days back in time, with a spatial resolution of 1° latitude by 1° longitude.

We further use several methane flux estimates to account for multiple different methane source types in the atmospheric modeling simulations. Specifically, we use the US EPA gridded methane emissions inventory across CONUS (Maasakkers et al. 2016) and the Emission Database for Global Atmospheric Research (EDGAR) gridded methane emissions version 5 (Crippa et al. 2019) for anthropogenic fluxes outside CONUS. Maasakkers et al. (2021) argue that the EPA inventory underestimates oil and gas emissions but that emissions from other anthropogenic sectors in the US are roughly consistent with atmospheric observations. Hence, we scale US oil production emissions by a factor of 1.59 and gas production emissions by 1.33 to match the inverse modeling estimate of Maasakkers et al. (2021). We additionally use wetland methane fluxes calculated using the model in Pickett-Heaps et al. (2011) (and as used in Miller et al. 2014, 2016). Several atmospheric modeling studies have argued that the wetland flux model from Pickett-Heaps et al. (2011) has a magnitude and spatiotemporal distribution that is generally consistent with in-situ atmospheric methane observations across Canada and the northern US (Miller et al. 2014, 2016; Pickett-Heaps et al. 2011). We further use biomass burning methane fluxes from the Quick Fire Emissions Dataset (QFED v2.4, Darmenov & da Silva, 2013). Maasakkers et al. (2021) find that the overall magnitude of QFED emissions is generally consistent with GOSAT observations. Each of these fluxes are regridded to a 1° latitude by 1° longitude spatial resolution for the atmospheric modeling simulations, though the native spatial resolution of these flux products is higher. Furthermore, anthropogenic and wetland fluxes have a monthly time resolution while QFED has a daily time resolution.

2.2 Modeling scenarios and trend fitting

We create two emissions scenarios (one with an emissions trend and one without an emissions trend) and two meteorology scenarios (one with IAV in meteorology and one without). In total, we analyze four modeling scenarios: with trends in emissions and IAV in meteorology (scenario 1), with trends in emissions and without IAV in meteorology (scenario 2), no trends in emissions and with IAV in meteorology (scenario 3), and no trends in emissions and without IAV in meteorology (scenario 4).

The emissions scenarios are generated based on the methane flux estimates described in Sect. 2.1. For the scenario with no emissions trend, we use the monthly US EPA inventory estimate for year 2012 in all years of the WRF-STILT model simulations. Similarly, we use monthly wetland fluxes and daily QFED fluxes also for year 2012. For the scenario with an emissions trend, we scale oil and gas emissions in each state relative to monthly U.S. dry natural gas production data (US EIA, 2018) from years 2007 to 2015. At the time of writing, emissions from the US EPA gridded inventory are only available for year 2012, and we scale oil and gas emissions up or down relative to 2012 inventory numbers. For the simulations here, we do not add a trend to other methane source types because we are primarily interested in how a plausible trend in oil and gas emissions would manifest at the atmospheric observation sites, all else being constant. Some recent studies argue that US methane emissions trends are likely being driven by the oil and gas sectors (e.g., Sheng et al. 2018, Turner et al. 2016), and we therefore create a hypothetical emissions scenario that focuses on that sector.

We further generate meteorology scenarios that include IAV in meteorology and scenarios that do not include IAV in meteorology. For the former scenarios, we run WRF-STILT using standard protocols as described in Sect. 2.1. For the latter scenarios, we average footprints from different years to remove IAV in meteorology. Specifically, at each in-situ monitoring site, we average the footprints from each month of the year across all years of modeling simulations. In other words, we average the WRF-STILT footprints from all Januarys (across 2007-2015), across all Februarys, etc. This approach preserves seasonal variability in the footprints but removes IAV. For the GOSAT observations, we group the observations into 4° latitude by 4° longitude grid boxes across the United States. Within each box, we average the footprints from each month as described above.

We subsequently fit trend lines to the model outputs for each scenario. We can then compare and contrast the impact of meteorology versus emissions on apparent trends in MMR. We specifically fit trend lines using the procedures outlined in Lan et al. (2019) for in situ observations and Sheng et al. (2018) for GOSAT observations. We use line-fitting procedures from these studies to ensure that the results presented here are directly comparable to existing research and to ensure that any differences from these existing studies are not due to differences in the trend-fitting procedure. Technical details of trend line fitting can be found in the SI Sect. S1.

3 Results and discussion

3.1 Meteorology yields an upward trend in atmospheric methane across the United States

We find that meteorology has a large impact on inter-annual variability (IAV) in modeled methane mixing ratios. For example, we calculate the maximum and minimum values in annually-averaged MMR at each observation site in the NOAA Global Monitoring Laboratory tall tower network. For these calculations, we use anthropogenic emissions that do not contain any trend (e.g., scenario 3 described above), such that IAV in MMR does not reflect variability in emissions. In these simulations, we find, on average, that IAV in MMR at the observation sites is equal to 40% of the total average atmospheric methane signal from North America (Fig. S1 – S8). At some sites, particularly sites that are close to large agricultural or oil and gas emissions sources, this IAV is as high as 59% of the average MMR (e.g., at Eerie, Colorado, site BAO). By contrast, at sites that are distant from large methane emissions, this IAV can be as small as 20% of the average MMR (e.g., at Argyle, Maine, site AMT).

In fact, IAV in meteorology also yields an apparent upward trend in MMR at all of the tall tower observation sites. Figure 1 displays the results of the four modeling scenarios at these sites. The individual bars in the plot display the trend (i.e., percent annum change) in MMR at each observation site estimated using a linear regression (Sect. 2). Specifically, the yellow bars display the results for scenarios that include a plausible upward trend in emissions while the blue bars display the results for scenarios that do not include a trend in emissions. Furthermore, dark-shaded bars display results for scenarios that include IAV in meteorology while light-shaded bars show scenarios where IAV in meteorology has been removed (Sect. 2). Note that we estimate negative trends at a few sites in a few scenarios. In most cases, the standard error bars encompass zero. In two other instances (S2 at STR and WGC), the negative trend estimate occurs at sites that have a very large seasonal cycle in MMR and have sustained data gaps; the combination makes trend estimation at these sites prone to error (discussed in Sect. S2).

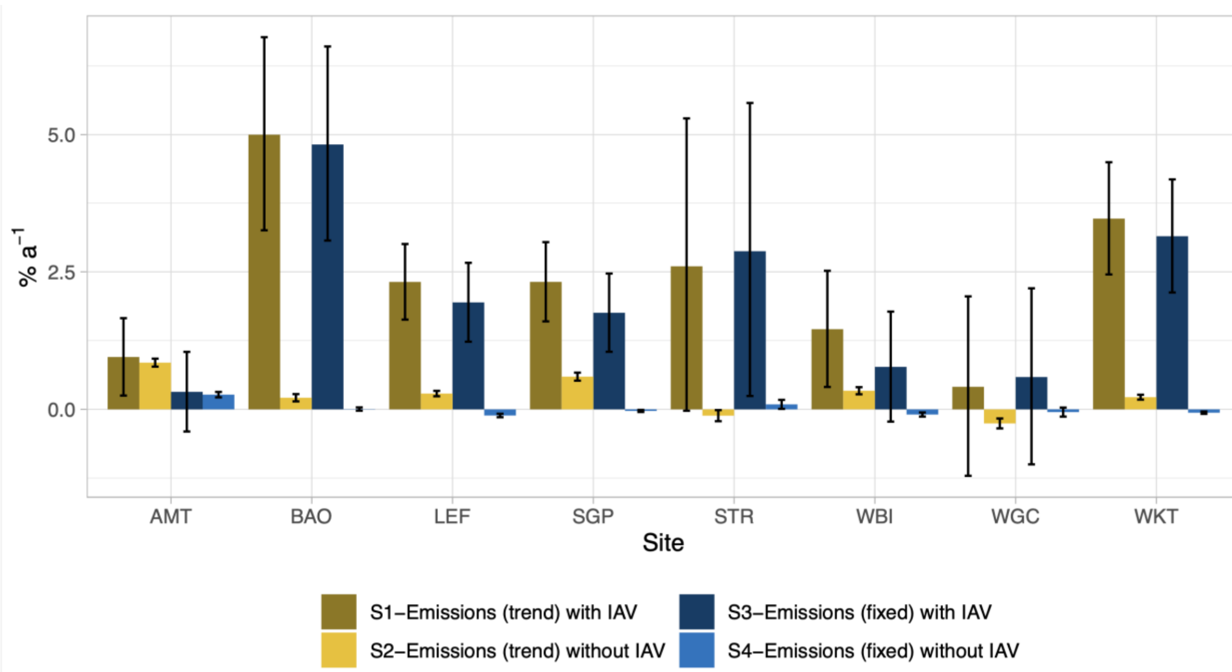

Figure 1. Estimated trends with uncertainty in MMR at different in-situ observation sites (years 2007-2015) and for different modeling scenarios. Sites include Argyle, Maine (AMT); Erie, Colorado (BAO); Park Falls, Wisconsin (LEF); Billings, Oklahoma (SGP); Sutro Tower, San Francisco, California (STR); West Branch, Iowa (WBI), Walnut Grove, California (WGC), and Moody, Texas (WKT) (Andrews et al. 2014). We find that IAV in meteorology has a much larger impact on estimated trends than does variability in emissions. Note that Figs. S1-S8 display the trends in observed MMR at these sites for reference.

We find an upward trend in MMR at all sites, irrespective of whether we include a trend in emissions (e.g., scenarios S1 and S3). By contrast, when we remove IAV in meteorology, the upward trend in MMR largely disappears (e.g., scenarios S2 and S4). We therefore conclude that meteorology is likely driving the trend in model outputs. Furthermore, even when we do not include a trend in emissions, the trend in the model outputs is often between 2-4% per annum and ranges from 0.2% per annum (at Argyle) to 5.5% per annum (at Erie) (scenario 3). These numbers are comparable in magnitude to the US methane emissions trend estimated by several recent atmospheric studies (e.g., Sheng et al. 2018, Turner et al. 2016). These studies attribute trends in observed atmospheric mixing ratios to emissions, while our results suggest that IAV in meteorology can yield comparable trends.

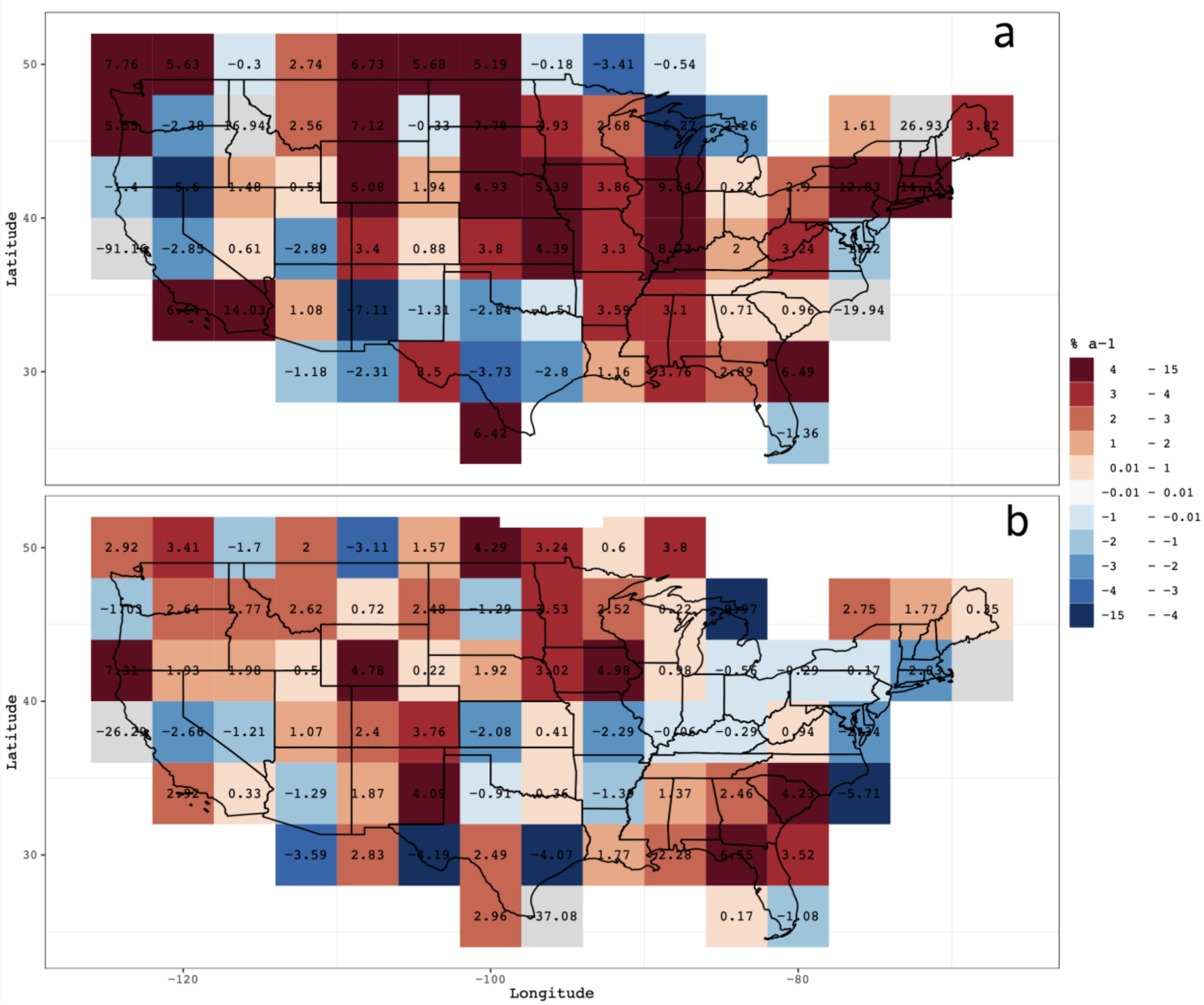

Figure 2. Estimated trends in MMR at GOSAT observation sites (years 2009-2015). Panel (a) displays the result of modeling scenario 3 (IAV in meteorology and no trend in emissions), while panel (b) displays the estimated trend in GOSAT observations. The modeled trend (a) has a similar overall magnitude to the observed trend (b), even though the former does not contain an emissions trend. Note that Fig. S18 – S21 display modeled trends for the three remaining scenarios not shown here.

By contrast, we find that plausible trends in emissions have a smaller impact on estimated trends in MMR relative to meteorology. For example, scenarios 1 and 3 in Fig. 1 display the results when we do and do not, respectively, include a plausible trend in anthropogenic emissions. The differences in estimated trends between these two scenarios is generally small; the difference is between 0.5 - 1.1% per annum, except at Argyle, a remote site in northern

Maine far from large emissions sources. In other words, the impact of an emissions trend is small relative to the overall trend in MMR.

Note that we conduct two sensitivity tests for observation sites in oil and gas producing regions (SGP and WKT) – one test that explores the impact of the meteorological product used in STILT and one that explores the impact of observation sampling time and frequency (Figs. S35-36). In simulations using both meteorology products, the impact of a trend in emissions is small relative to IAV due to meteorology, though the models do not always agree on the exact magnitude of MMR in specific months. In the second test, we find that variations in sampling time have little impact on MMR at one site (WKT) but do impact the results at another site (SGP); hence, we cannot rule out the role of observation sampling frequency and time on estimates of atmospheric methane trends.

We find similar results for simulated GOSAT methane observations. Figure 2 displays the estimated trend in MMR from scenario 3 (panel a) and from the GOSAT observations (panel b) (Fig. S18, S19, and S21 displays scenarios 1, 2, and 4.). The figure shows the trend (% per annum) for model outputs and observations aggregated into 4° by 4° latitude-longitude grid boxes (Sect. 2). The model simulations shown here do not include a trend in emissions, yet the overall trend in MMR is roughly comparable in magnitude to the overall trend in the GOSAT observations. Thus, it is plausible that variability in meteorology is driving much of the observed trend in GOSAT observations. Note that a small number of grid boxes yield unrealistic trend estimates (e.g., coastal northern California and northern Vermont). These grid boxes contain a limited number of observations that are not evenly distributed across seasons and years during the study period, making trend estimation challenging. Also note that Figs. S22-S28 display detailed modeled and observation time series at several prototypical locations across the United States.

We note that the results described above could differ if analyzed across a longer time horizon (e.g., across multiple decades). If there were sustained emissions trends across multiple decades, it might be easier to identify directly from atmospheric observations, even given large IAV in meteorology. With that said, existing studies of methane trends have examined similar time periods to this study (e.g., Lan et al. 2019, Maasakkers et al. 2020, Sheng et al. 2018, Turner et al. 2016). Furthermore, observations that span multiple decades are rarely available, except at a handful of global monitoring sites (at the time of writing), and shorter time periods, like those evaluated in this study, are also helpful for evaluating the impacts of emissions policies in a timely manner (e.g., Miller et al. 2019).

3.2 Local meteorological processes correlate with atmospheric methane trends

In Sect. 3.1, we argue that meteorology yields large IAV in MMR, and a natural follow-up question is to evaluate what specific aspects of meteorology correlate with this IAV. We find that IAV in local meteorological processes show a strong correlation with IAV in MMR. To evaluate this question, we examine the correlation between annually-averaged MMR and the "local" STILT footprint. The STILT footprint estimates the impact of emissions in a given location on the observation site (in units of ppb per unit emission). Here, we define the local footprint as the 1° latitude/longitude grid box where the observation is located, and we then average this footprint across each year. We compare these local footprints against annually-averaged MMR. Figure 3 displays the results of this analysis for model outputs at GOSAT observation locations (panel a) and in situ observation locations (panel b). We find that the correlation (r) between MMR and the local footprint is strong -- greater than 0.8 in many locations for the GOSAT simulations and greater than 0.5 at most locations. The correlation is similarly strong for the simulations at in situ observation sites -- between 0.8 and 1.0.

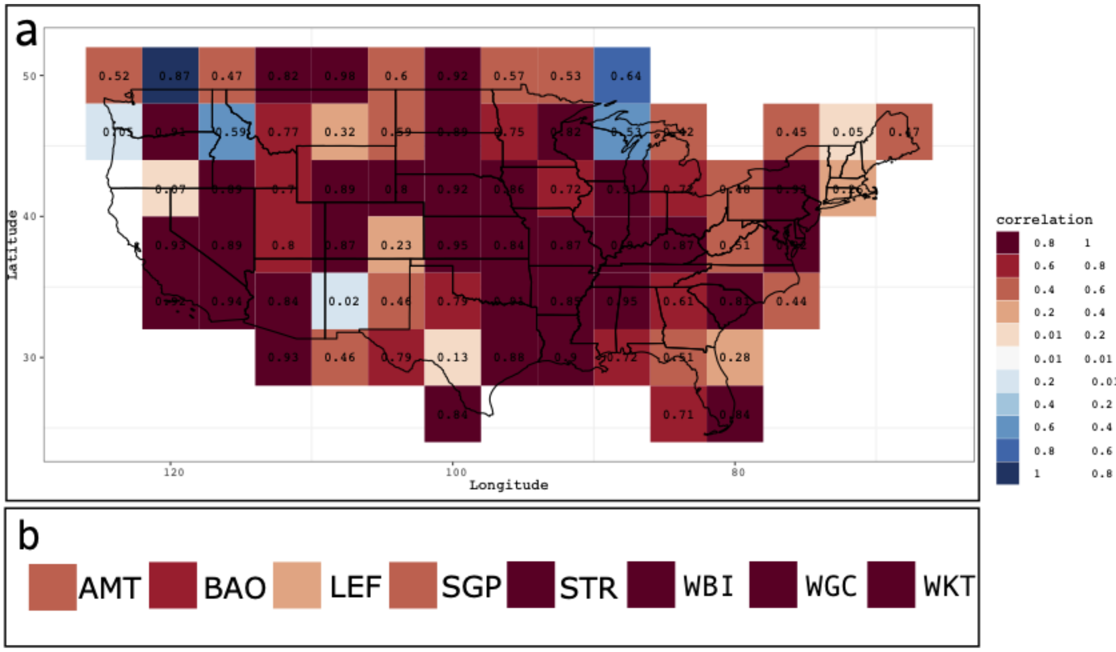

Figure 3. The correlation (*r*) between annually-averaged MMR and the local footprint (Sect. 3.2), both at GOSAT and in-situ observation locations. We find a close correlation at most locations, suggesting that local meteorological processes play a key role in IAV of MMR.

We further explore the relationships between IAV in MMR and IAV in several specific, local meteorological processes -- including planetary boundary layer (PBL) height, vertical wind speed (Ω), and total wind speed at the observation location and modeling height (i.e., the Euclidean sum of u and v wind speed). In this specific study, we use estimates for these parameters from North American Regional Reanalysis (NARR, NCEP, 2005). At the in situ observation sites, we often find the strongest anti-correlations between IAV in MMR and IAV in annually-averaged local wind speed, particularly at sites near large sources (e.g., WGC and WKT). When local winds are stagnant, methane (presumably from local sources) accumulates around the observation site. By contrast, faster winds likely promote greater ventilation and thereby decrease methane at the observation sites. Urban sites (e.g., STR, BAO), however, exhibit a stronger anti-correlation with PBL height. At these sites, larger PBL heights are associated with dilution of the urban pollution dome. Curiously, MMR at two sites (LEF, AMT) is positively correlated with PBL height. At these remote sites, higher PBL heights could be associated with greater transport of methane from distant source regions.

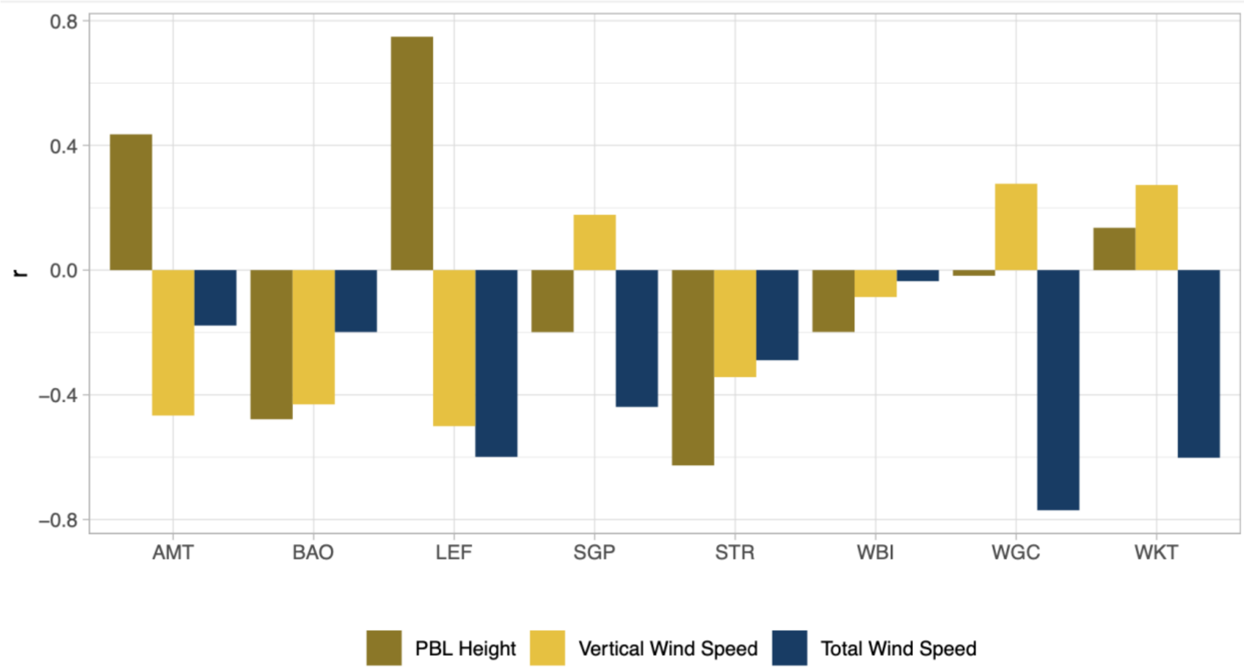

Figure 4. The correlation (*r*) between annually-averaged MMR and various meteorological factors at the in-situ observation sites. We find that MMR is often anti-correlated with local wind speed, though the strength of that relationship varies by site. By contrast, at urban sites (STR and BAO), we find the strongest anti-correlation with PBL height.

Note that we are not able to identify meaningful correlations between IAV in MMR and specific meteorological parameters for the GOSAT simulations. GOSAT observes methane mixing ratios across an entire vertical atmospheric column. As a result, IAV in MMR is likely influenced by a complex mixture of meteorological parameters across different altitudes.

Our findings on methane trends are in parallel with several other studies that report on the role of atmospheric transport in air pollutant and GHG variability (e.g., Keppel-Aleks et al. 2011, Kerr et al. 2020, 2021, Samaddar et al. 2021, Torres et al. 2019). These studies generally find that transport plays a dominant role in explaining meso- and synoptic-scale variability in trace gas mixing ratios. For example, Keppel-Aleks et al. (2011) report that variations in total column CO_2 mixing ratios are forced both by local CO_2 fluxes and advection on diurnal scales, and on synoptic scales, CO_2 variations arise due to large-scale eddy-driven disturbances of the meridional gradient. Torres et al. (2019) report similar findings using CO_2 observations from the Orbiting Carbon Observatory 2 (OCO-2). Kerr et al. (2020, 2021) further argue that daily, continental-scale variations of O_3 are largely meteorology driven and are influenced by the meridional flow related to the jet stream. In the present study, we also find that transport plays a dominant role in trace gas (i.e., CH_4) mixing ratios, albeit at annual instead of the daily/synoptic scales examined in the aforementioned studies.

4 Conclusions

Natural gas production activities in the US increased during the shale gas boom, leading to concerns about increasing methane emissions. In fact, several studies report increasing MMR across the US relative to the global mean. However, we find that meteorology, not emissions, can explain this upward trend MMR between 2007 and 2015. We then explore which meteorological factors correlate with this upward trend. Using a footprint analysis, we argue that IAV in MMR is likely correlated with local meteorological processes. At in situ monitoring sites, we also find higher correlations between MMR and IAV in local wind speed than with meteorological parameters related to vertical mixing.

Overall, our results show that IAV in MMR reflect variability in meteorology as much or more than variability in emissions. This finding poses an inherent challenge for detecting trends in emissions because, at least in the case of methane, the atmospheric signal of that emissions trend is comparatively small. This result is especially applicable given the limited time span of many existing in situ and satellite observation records. This study further cautions against interpreting trends in atmospheric greenhouse gas mixing ratios as a direct proxy for trends in emissions.

This work also lends support for existing studies that show little or no trend in US methane emissions. Specifically, existing studies fall into two categories: studies that directly interpret trends in atmospheric observations (e.g., Lan et al. 2019, Sheng et al. 2018,Turner et al. 2016) and studies that estimate emissions using inverse modeling, which accounts for meteorology using a modeled and/or reanalysis product (e.g., Benmergui et al. 2015, Lu et al. 2021, Maasakers et al. 2020). Studies that directly interpret trends from atmospheric observations find an upward emissions trend during a similar time period as the present study (2.5 - 4.7% per annum). By contrast, studies that account for atmospheric transport through the use of inverse modeling find little upward trend in methane emissions (e.g., 0.1 - 0.7% per annum). Inverse modeling studies account for trends in MMR due to meteorology instead of aliasing the trends on emissions, and the present studies therefore helps explain these seemingly irreconcilable results.

Acknowledgments

This work was funded by a Johns Hopkins University Discovery Grants. The authors declare no conflicts of interest. We thank Thomas Nehrkorn and Marikate Mountain from AER, Inc. for generating STILT footprints.

Open Research

The in situ observations used in this study are available from the NOAA Global Monitoring Laboratory ObsPack (Cooperative Global Atmospheric Data Integration Project 2020). The GOSAT methane observations (UoL Proxy XCH_4 Retrieval Version 9) are available at http://dx.doi.org/10.5285/18ef8247f52a4cb6a14013f8235cc1eb. In addition, STILT footprints from CarbonTracker-Lagrange are available at https://gml.noaa.gov/ccgg/carbontracker-lagrange/.

References

Andrews, A. E., Kofler, J. D., Trudeau, M. E., Williams, J. C., Neff, D. H., Masarie, K. A., et al. (2014). CO_2, CO, and CH_4 measurements from tall towers in the NOAA Earth System Research Laboratory's Global Greenhouse Gas Reference Network: Instrumentation, uncertainty analysis, and recommendations for future high-accuracy greenhouse gas monitoring efforts. *Atmospheric Measurement Techniques*, *7*(2), 647-687. https://doi.org/10.5194/amt-7-647-2014

Alvarez, R. A., Zavala-Araiza, D., Lyon, D. R., Allen, D. T., Barkley, Z. R., Brandt, A. R.,et al. (2018). Assessment of methane emissions from the US oil and gas supply chain. *Science*, *361*(6398), 186-188. https://doi.org/10.1126/science.aar7204

Barkley, Z. R., Davis, K. J., Feng, S., Cui, Y. Y., Fried, A. L. A. N., Weibring, P. E. T. T. E. R., et al. (2021). Analysis of Oil and Gas Ethane and Methane Emissions in the Southcentral and Eastern United States Using Four Seasons of Continuous Aircraft Ethane Measurements. *Journal of Geophysical Research: Atmospheres*, *126*(10), e2020JD034194. https://doi.org/10.1029/2020JD034194

Barkley, Z. R., Lauvaux, T., Davis, K. J., Deng, A., Fried, A., Weibring, P., et al. (2019). Estimating methane emissions from underground coal and natural gas production in Southwestern Pennsylvania. *Geophysical Research Letters*, *46*(8), 4531-4540. https://doi.org/10.1029/2019GL082131

Benmergui, J. S., Andrews, A. E., Thoning, K. W., Trudeau, M., Miller, S. M., Dlugokencky, E. J., et al. (2015,). Integrating diverse observations of North American CH_4 into flux inversions in CarbonTrackerLagrange-CH_4. In *AGU Fall Meeting Abstracts* (Vol. 2015, pp. A33F-0245).

Brandt, A. R., Heath, G. A., & Cooley, D. (2016). Methane Leaks from Natural Gas Systems Follow Extreme Distributions. *Environmental Science & Technology*, *50*(22), 12512-12520. https://doi.org/10.1021/acs.est.6b04303

Caulton, D. R., Lu, J. M., Lane, H. M., Buchholz, B., Fitts, J. P., Golston, L. M., et al. (2019). Importance of Superemitter Natural Gas Well Pads in the Marcellus Shale. *Environmental Science & Technology*, *53*(9), 4747-4754. https://doi.org/10.1021/acs.est.8b06965

Cleveland, R. B., Cleveland, W. S., and Terpenning, I.: STL: A seasonal-trend Decomposition Procedure Based on Loess, *Journal of Official Statistics*, *6*, 3–73, 1990.

Crippa, M., Oreggioni, G., Guizzardi, D., Muntean, M., Schaaf, E., Lo Vullo, E., et al. (2019). Fossil CO_2 and GHG emissions of all world countries - 2019 Report, *EUR 29849 EN*, Publications Office of the European Union, Luxembourg, 2019, ISBN 978-92-76-11100-9, https://doi.org/10.2760/687800

Cooperative Global Atmospheric Data Integration Project; (2020): Multi-laboratory compilation of atmospheric methane data for the period 1957-2018;

obspack_ch4_1_GLOBALVIEWplus_v2.0_2020-04-24 [Dataset]; NOAA Earth System Research Laboratory, Global Monitoring Division. http://dx.doi.org/10.25925/20200424

Cui, Y. Y., Brioude, J., Angevine, W. M., Peischl, J., McKeen, S. A., Kim, S. W., et al. (2017). Top-down estimate of methane emissions in California using a mesoscale inverse modeling technique: The San Joaquin Valley. *Journal of Geophysical Research: Atmospheres*, *122*(6), 3686-3699. https://doi.org/10.1002/2016JD026398

Cui, Y. Y., Brioude, J., McKeen, S. A., Angevine, W. M., Kim, S. W., Frost, G. J., et al. (2015). Top-down estimate of methane emissions in California using a mesoscale inverse modeling technique: The South Coast Air Basin. *Journal of Geophysical Research: Atmospheres*, *120*(13), 6698-6711. https://doi.org/10.1002/2014JD023002

Darmenov, A. & da Silva, A. (2013). *The quick fire emissions dataset (QFED)–documentation of versions 2.1, 2.2 and 2.4, NASA Technical Report Series on Global Modeling and Data Assimilation, NASA TM-2013-104606*. (Vol. 38). https://ntrs.nasa.gov/api/citations/20180005253/downloads/20180005253.pdf

Goldstein, A. H., Wofsy, S. C., & Spivakovsky, C. M. (1995). Seasonal variations of nonmethane hydrocarbons in rural New England: Constraints on OH concentrations in northern midlatitudes. *Journal of Geophysical Research: Atmospheres*, 100(D10), 21023-21033. https://doi.org/10.1029/95JD02034

Howarth, R. W. (2019). Ideas and perspectives: is shale gas a major driver of recent increase in global atmospheric methane?. *Biogeosciences, 16*(15), 3033-3046. https://doi.org/10.5194/bg-16-3033-2019

Hu, L., Andrews, A. E., Thoning, K. W., Sweeney, C., Miller, J. B., Michalak, A. M., et al. (2019). Enhanced North American carbon uptake associated with El Niño. *Science Advances, 5*(6), eaaw0076. https://doi.org/10.1126/sciadv.aaw0076

Huang, Y., Kort, E. A., Gourdji, S., Karion, A., Mueller, K., & Ware, J. (2019). Seasonally resolved excess urban methane emissions from the Baltimore/Washington, DC metropolitan region. *Environmental Science & Technology*, *53*(19), 11285-11293. https://doi.org/10.1021/acs.est.9b02782

Jeong, S., Hsu, Y. K., Andrews, A. E., Bianco, L., Vaca, P., Wilczak, J. M., et al. (2013). A multitower measurement network estimate of California's methane emissions. *Journal of Geophysical Research: Atmospheres*, *118*(19), 11-339. https://doi.org/10.1002/jgrd.50854

Keppel-Aleks, G., Wennberg, P. O., & Schneider, T. (2011). Sources of variations in total column carbon dioxide. *Atmospheric Chemistry and Physics*, 11(8), 3581-3593. https://doi.org/10.5194/acp-11-3581-2011

Kerr, G. H., Waugh, D. W., & Miller, S. M. (2021). Jet Stream-Surface Tracer Relationships: Mechanism and Sensitivity to Source Region. *Geophysical Research Letters*, 48(1), e2020GL090714. https://doi.org/10.1029/2020GL090714

Kerr, G. H., Waugh, D. W., Steenrod, S. D., Strode, S. A., & Strahan, S. E. (2020). Surface Ozone-Meteorology Relationships: Spatial Variations and the Role of the Jet Stream. *Journal of Geophysical Research: Atmospheres*, 125(21), e2020JD032735. https://doi.org/10.1029/2020JD032735

Lan, X., Tans, P., Sweeney, C., Andrews, A., Dlugokencky, E., Schwietzke, S., et al. (2019). Long-term measurements show little evidence for large increases in total US methane emissions over the past decade. *Geophysical Research Letters*, *46*(9), 4991-4999. https://doi.org/10.1029/2018GL081731

Lin, J. C., Gerbig, C., Wofsy, S. C., Andrews, A. E., Daube, B. C., Davis, K. J., et al. (2003). A near-field tool for simulating the upstream influence of atmospheric observations: The Stochastic Time-Inverted Lagrangian Transport (STILT) model. *Journal of Geophysical Research: Atmospheres*, *108*(D16). https://doi.org/10.1029/2002JD003161

Lu, X., Jacob, D. J., Wang, H., Maasakkers, J. D., Zhang, Y., Scarpelli, T. R., et al. (2021). Methane emissions in the United States, Canada, and Mexico: Evaluation of national methane emission inventories and sectoral trends by inverse analysis of in situ (GLOBALVIEWplus CH_4 ObsPack) and satellite (GOSAT) atmospheric observations. *Atmospheric Chemistry and Physics Discussions*, 1-41. https://doi.org/10.5194/acp-22-395-2022

Maasakkers, J. D., Jacob, D. J., Sulprizio, M. P., Scarpelli, T. R., Nesser, H., Sheng, J., et al. (2021). 2010–2015 North American methane emissions, sectoral contributions, and trends: a high-resolution inversion of GOSAT observations of atmospheric methane. *Atmospheric Chemistry and Physics*, *21*(6), 4339-4356. https://doi.org/10.5194/acp-21-4339-2021

Maasakkers, J. D., Jacob, D. J., Sulprizio, M. P., Turner, A. J., Weitz, M., Wirth, T., et al. (2016). Gridded national inventory of US methane emissions. *Environmental Science & Technology*, *50*(23), 13123-13133. https://doi.org/10.1021/acs.est.6b02878

Miller, S. M., Andrews, A. E., Benmergui, J., Commane, R., Dlugokencky, E. J., Janssens-Maenhout, G., et al. (2015). The ability of atmospheric data to resolve discrepancies in wetland methane estimates over North America. *Biogeosciences Discussions*, 12(23). https://doi.org/10.5194/bgd-12-9341-2015

Miller, S. M., Commane, R., Melton, J. R., Andrews, A. E., Benmergui, J., Dlugokencky, E. J., et al. (2016). Evaluation of wetland methane emissions across North America using atmospheric data and inverse modeling. *Biogeosciences*, *13*(4), 1329-1339. https://doi.org/10.5194/bg-13-1329-2016

Miller, S. M., Michalak, A. M., Detmers, R. G., Hasekamp, O. P., Bruhwiler, L. M., & Schwietzke, S. (2019). China's coal mine methane regulations have not curbed growing emissions. *Nature Communications*, *10*(1), 1-8. https://doi.org/10.1038/s41467-018-07891-7

Miller, S. M., Miller, C. E., Commane, R., Chang, R. Y. W., Dinardo, S. J., Henderson, J. M., et al. (2016). A multiyear estimate of methane fluxes in Alaska from CARVE atmospheric observations. *Global Biogeochemical Cycles*, *30*(10), 1441-1453. https://doi.org/10.1002/2016GB005419

Miller, S. M., Wofsy, S. C., Michalak, A. M., Kort, E. A., Andrews, A. E., Biraud, S. C., et al. (2013). Anthropogenic emissions of methane in the United States. *Proceedings of the National Academy of Sciences*, *110*(50), 20018-20022. https://doi.org/10.1073/pnas.1314392110

Miller, S. M., Worthy, D. E., Michalak, A. M., Wofsy, S. C., Kort, E. A., Havice, T. C., et al. (2014). Observational constraints on the distribution, seasonality, and environmental predictors of North American boreal methane emissions. *Global Biogeochemical Cycles*, *28*(2), 146-160. https://doi.org/10.1002/2013GB004580

Nehrkorn, T., Eluszkiewicz, J., Wofsy, S. C., Lin, J. C., Gerbig, C., Longo, M., at al. (2010). Coupled weather research and forecasting–stochastic time-inverted lagrangian transport (WRF–STILT) model. *Meteorology and Atmospheric Physics*, *107*(1), 51-64. https://doi.org/10.1007/s00703-010-0068-x

National Centers for Environmental Prediction/National Weather Service/NOAA/U.S. Department of Commerce. (2005). NCEP North American Regional Reanalysis (NARR) [Dataset]. Research Data Archive at the National Center for Atmospheric Research, Computational and Information Systems Laboratory. https://rda.ucar.edu/datasets/ds608.0

National Centers for Environmental Prediction/National Weather Service/NOAA/U.S. Department of Commerce, (2015): NCEP North American Mesoscale (NAM) 12 km Analysis [Dataset]. Research Data Archive at the National Center for Atmospheric Research, Computational and Information Systems Laboratory, Boulder, CO. https://doi.org/10.5065/G4RC-1N91

Omara, M., Zimmerman, N., Sullivan, M. R., Li, X., Ellis, A., Cesa, R., et al. (2018). Methane emissions from natural gas production sites in the United States: Data synthesis and national estimate. *Environmental Science & Technology*, *52*(21), 12915-12925. https://doi.org/10.1021/acs.est.8b03535

Parker, R. J., Webb, A., Boesch, H., Somkuti, P., Barrio Guillo, R., Di Noia, A., et al. (2020). A decade of GOSAT Proxy satellite CH_4 observations, *Earth System Science Data, 12,* 3383–3412. https://doi.org/10.5194/essd-12-3383-2020, 2020

Pickett-Heaps, C. A., Jacob, D. J., Wecht, K. J., Kort, E. A., Wofsy, S. C., Diskin, G. S., et al. (2011). Magnitude and seasonality of wetland methane emissions from the Hudson Bay

Lowlands (Canada). *Atmospheric Chemistry and Physics*, *11*(8), 3773-3779. https://doi.org/10.5194/acp-11-3773-2011

Rella, C. W., Tsai, T. R., Botkin, C. G., Crosson, E. R., & Steele, D. (2015). Measuring emissions from oil and natural gas well pads using the mobile flux plane technique. *Environmental Science & Technology*, *49*(7), 4742-4748. https://doi.org/10.1021/acs.est.5b00099

Ren, X., Salmon, O. E., Hansford, J. R., Ahn, D., Hall, D., Benish, S. E., et al. (2018). Methane emissions from the Baltimore-Washington area based on airborne observations: Comparison to emissions inventories. *Journal of Geophysical Research: Atmospheres*, *123*(16), 8869-8882. https://doi.org/10.1029/2018JD028851

Robertson, A. M., Edie, R., Field, R. A., Lyon, D., McVay, R., Omara, M., et al. (2020). New Mexico Permian Basin measured well pad methane emissions are a factor of 5–9 times higher than US EPA estimates. *Environmental Science & Technology*, *54*(21), 13926-13934. https://doi.org/10.1021/acs.est.0c02927

Samaddar, A., Feng, S., Lauvaux, T., Barkley, Z. R., Pal, S., & Davis, K. J. (2021). Carbon dioxide distribution, origins, and transport along a frontal boundary during summer in mid-latitudes. *Journal of Geophysical Research: Atmospheres*, 126(9), e2020JD033118. https://doi.org/10.1029/2020JD033118

Saunois, M., Stavert, A. R., Poulter, B., Bousquet, P., Canadell, J. G., Jackson, R. B., et al. (2020). The global methane budget 2000–2017. *Earth System Science Data*, *12*(3), 1561-1623. https://doi.org/10.5194/essd-12-1561-2020

Sargent, M. R., Floerchinger, C., McKain, K., Budney, J., Gottlieb, E. W., Hutyra, L. R., et al. (2021). Majority of US urban natural gas emissions unaccounted for in inventories. *Proceedings of the National Academy of Sciences*, *118*(44). https://doi.org/10.1073/pnas.2105804118

Sheng, J. X., Jacob, D. J., Turner, A. J., Maasakkers, J. D., Benmergui, J., Bloom, A. A., et al. (2018). 2010–2016 methane trends over Canada, the United States, and Mexico observed by the GOSAT satellite: contributions from different source sectors. *Atmospheric Chemistry and Physics*, *18*(16), 12257-12267. https://doi.org/10.5194/acp-18-12257-2018

Shiga, Y. P., Michalak, A. M., Fang, Y., Schaefer, K., Andrews, A. E., Huntzinger, D. H., et al. (2018). Forests dominate the interannual variability of the North American carbon sink. *Environmental Research Letters*, *13*(8), 084015. http://dx.doi.org/10.1088/1748-9326/aad505

Shiga, Y. P., Tadić, J. M., Qiu, X., Yadav, V., Andrews, A. E., Berry, J. A., et al. (2018). Atmospheric CO_2 observations reveal strong correlation between regional net biospheric carbon uptake and solar-induced chlorophyll fluorescence. *Geophysical Research Letters*, *45*(2), 1122-1132. https://doi.org/10.1002/2017GL076630

Skamarock, W. C., Klemp, J. B., Dudhia, J., Gill, D. O., Barker, D. M., Wang, W., at al. (2008). A description of the Advanced Research WRF version 3. *NCAR Technical note-475+ STR*. https://doi.org/10.5065/D68S4MVH

Torres, A. D., Keppel-Aleks, G., Doney, S. C., Fendrock, M., Luis, K., & Wunch, D. (2019). A geostatistical framework for quantifying the imprint of mesoscale atmospheric transport on satellite trace gas retrievals. *Journal of Geophysical Research: Atmospheres*, 124(17-18), 9773-9795. https://doi.org/10.1029/2018JD029933

Turner, A. J., Jacob, D. J., Benmergui, J., Wofsy, S. C., Maasakkers, J. D., Butz, A., et al. (2016). A large increase in US methane emissions over the past decade inferred from satellite data and surface observations. *Geophysical Research Letters*, *43*(5), 2218-2224. https://doi.org/10.1002/2016GL067987

United States Energy Information Administration (2016). Hydraulically fractured wells provide two-thirds of U.S. natural gas production. https://www.eia.gov/todayinenergy/detail.php?Id=26112

United States Energy Information Administration. (2018). Natural Gas Gross Withdrawals and Production [Dataset]. https://www.eia.gov/dnav/ng/ng_prod_sum_a_EPG0_FPD_mmcf_m.htm

United States Environmental Protection Agency (2021). Inventory of U.S. greenhouse gas emissions and sink. https://www.epa.gov/sites/default/files/2021-04/documents/us-ghg-inventory-2021-main-text.pdf?VersionId=yu89kg1O2qP754CdR8Qmyn4RRWc5iodZ

Zavala-Araiza, D., Alvarez, R. A., Lyon, D. R., Allen, D. T., Marchese, A. J., Zimmerle, D. J., et al. (2017). Super-emitters in natural gas infrastructure are caused by abnormal process conditions. *Nature Communications*, *8*(1), 1-10. https://doi.org/10.1038/ncomms14012

Zavala-Araiza, D., Lyon, D. R., Alvarez, R. A., Davis, K. J., Harriss, R., Herndon, S. C., et al. (2015). Reconciling divergent estimates of oil and gas methane emissions. *Proceedings of the National Academy of Sciences*, *112*(51), 15597-15602. https://doi.org/10.1073/pnas.1522126112

Geophysical Research Letter

Supporting Information for

Ambiguity in Recent Changes to US Methane Emissions

Leyang Feng[1], Sakineh Tavakkoli[2], Sarah M. Jordaan[2], Arlyn E. Andrews[3], Joshua S. Benmergui[4], Darryn W. Waugh[5], Mingyang Zhang[1], Dylan C. Gaeta[1], and Scot M. Miller[1]

[1]Department of Environmental Health and Engineering, Johns Hopkins University, Baltimore, MD

[2]School of Advanced International Studies, Johns Hopkins University, Washington, DC

[3]Global Monitoring Laboratory, Earth System Research Laboratories, NOAA, Boulder, CO

[4]John A. Paulson School of Engineering and Applied Sciences, Harvard University, Boston, MA

[5]Department of Earth & Planetary Sciences, Johns Hopkins University, Baltimore, MD

Contents of this file

Figures S29 - S35:	Scatter plot of total enhancement vs local footprints for GOSAT observations at 7 prototypical locations
Figures S36 - S37:	MMR timeseries comparison for WRF, NAM12, NAMs12-fixed meteorology products

S1 Additional details on trend line fitting for in-situ observations and GOSAT

This section of the supplement provides detailed steps of trend line fitting for in-situ and GOSAT observations using modeled MMR. Specifically, we fit trend lines at each in-situ observation site for each scenario. As in Lan et al. (2019), we fit a linear trend line using ordinary least squares (OLS) to monthly model estimates that have been deseasonalized using a 2nd-order polynomial fit and band pass filter. The data are further log10 transformed before line fitting (If the model output were to increase by a constant percentage per annum, the resulting output would have a non-linear slope, and the log10 transformation would make that slope linear.). For GOSAT, we first average the model output into 4° by 4° latitude-longitude grid boxes across CONUS and estimate a trend for each grid box, the same procedure as Sheng et al. (2018). GOSAT sounding locations are sparsely distributed and vary from month-to-month, and this averaging procedure yields a more consistent MMR estimate for each grid box. We deseasonalize the model outputs using seasonal-trend-loess (STL) decomposition method (Cleveland et al. 1990), and fit a trend-line to annually-averaged model outputs using OLS.

S2 Additional details on the analysis for in-situ monitoring sites

This section of the supplement provides additional analysis of the model outputs at in situ atmospheric monitoring sites: detailed model time series at each site, comparisons against trends in observed atmospheric mixing ratios, and additional comparisons against individual meteorological variables.

Figures S1 - S8 display time series of MMR at each in situ observation site and for each modeling scenario (i.e., scenarios 1-4). Each figure displays monthly-averaged model outputs that have been deseasonalized, as described in Sect. 2.2. In addition, the figures show the trend line fitted to the modeled time series for each scenario. The time series show a clear upward trend in MMR at most observation sites (at least for several model scenarios), providing a visual confirmation of the trend lines reported in Fig. 1

The figures further show observed methane enhancements (deseasonalized and interpolated for gap-filling, shown in black) and a trend line fitted to these observed enhancements. The model outputs often do a good job of reproducing monthly variability in the observations, even if the model outputs do not always match the magnitude of the observations. Note that the purpose of this study is not to determine which of the modeled scenarios is the best match against observations. Rather, the four scenarios developed here are used as test cases to explore the plausible impacts of meteorology and emissions. By contrast, trends in observed atmospheric methane are likely due to a combination of both meteorological factors and complex, unknown trends in surface emissions. We feel that the latter are best estimated using Bayesian inverse modeling, which is beyond the scope of this manuscript.

Note that in Figs. S1-S8, the fitted trend lines for observed methane enhancements (shown in black) for a few sites exhibits a slight downward trend (i.e., site BAO, WBI, and WGC). We find that such downward trends are likely due to a reduction in observation frequency. Figs. S9-S11 display the timeseries with fitted trend lines of observed, monthly-averaged methane enhancements (shown in black), deseasonalized observed methane enhancements (shown in blue), and monthly observation frequency (grey bars in the background). All three sites (BAO, WBI, and WGC) show a downward shift in the timeseries associated with a change in observation frequency: these timeseries show an upward trend before 2011 and after 2011 but exhibit a downward shift in 2011. Such reduction in observations can cause observation sites to capture less variability in atmospheric methane within a given month, especially sporadic methane spikes from nearby cities or other sources, and can result in fitting unrealistic downward trends.

Also note that the observed methane enhancements displayed in Figs. S1-S8 show mixing ratios after subtracting a modeled methane background or boundary condition. The methane boundary condition used here approximates methane mixing ratios in air over the Pacific and Atlantic Oceans before these air masses enter the United States. The purpose of this study is to explore methane trends across the US, not global trends, and subtracting the methane boundary condition removes the influence of global methane trends from the analysis. By contrast, we do not need to subtract a boundary condition from the model simulations; the STILT simulations here are regional in scope and only model atmospheric methane enhancements due to fluxes in North America.

We use the methane boundary condition generated for NOAA's CarbonTracker-Lagrange project for all simulations in this study. This approach is identical to that used in multiple existing methane and GHG modeling studies based on the STILT model (e.g., Hu et al. 2019; Miller et al. 2013, 2014, 2016; Shiga et al. 2018a, 2018b). Specifically, we first interpolate in situ methane observations zonally and in time to create an interpolated "curtain" of estimated methane values across the Pacific and Atlantic oceans (e.g., as in Jeong et al. 2013 and Miller et al. 2013). We then sample this curtain at the ending locations and times of the particles in each STILT simulation. For each STILT simulation, we then average the sampled curtain values across all 500 particles in the simulation, and this average value becomes the estimated background for a specific methane observation.

Further note that we do not include methane oxidation in either the methane boundary condition calculations or in the calculation of STILT footprints. This approach is similar to other studies of regional methane emissions that use a particle trajectory model like STILT (e.g., Cui et al. 2015, 2017; Huang et al. 2019; Miller et al. 2013, 2014, 2016a, 2016b; Ren et al. 2018; Sargent et al. 2021). The atmospheric lifetime of methane is 12 years, while the particles in each STILT simulation are allowed to travel backward in time for 10 days (though many trajectories terminate at the edge of the North American model domain in less time). Over 10 days, up to 0.2 – 0.3% of modeled methane could decay, and we therefore do not include this chemistry in model simulations due to its small impact. Furthermore, even large inter-annual variability in hydroxyl radical (OH) levels would likely have minimal impact on the model simulations here given their regional scope.

Figures S12 – S14 provide additional detail on the comparisons between annual-averaged, modeled MMR and various meteorological parameters (i.e., planetary boundary layer (PBL) height, vertical wind speed (Ω), and total wind speed at the observation location). These figures display each comparison as a scatterplot, whereas Fig. 4 in the main article lists the estimated correlation coefficient for each comparison. These figures provides visual confirmation that the comparison between MMR and local wind speed is often stronger than the comparisons between MMR and other meteorological parameters.

Figures S15 – S17 further compare observed methane enhancements against the meteorological parameters described above. Fig. 4 in the main article displays this comparison for modeled methane outputs while the figure here shows the same comparison for observed methane enhancements. Similar to the model analysis in Fig. 4, we also find that the relationships between observed methane enhancements and meteorology are often strongest for local wind speed. This result provides further confirmation of the analysis in Fig. 4.

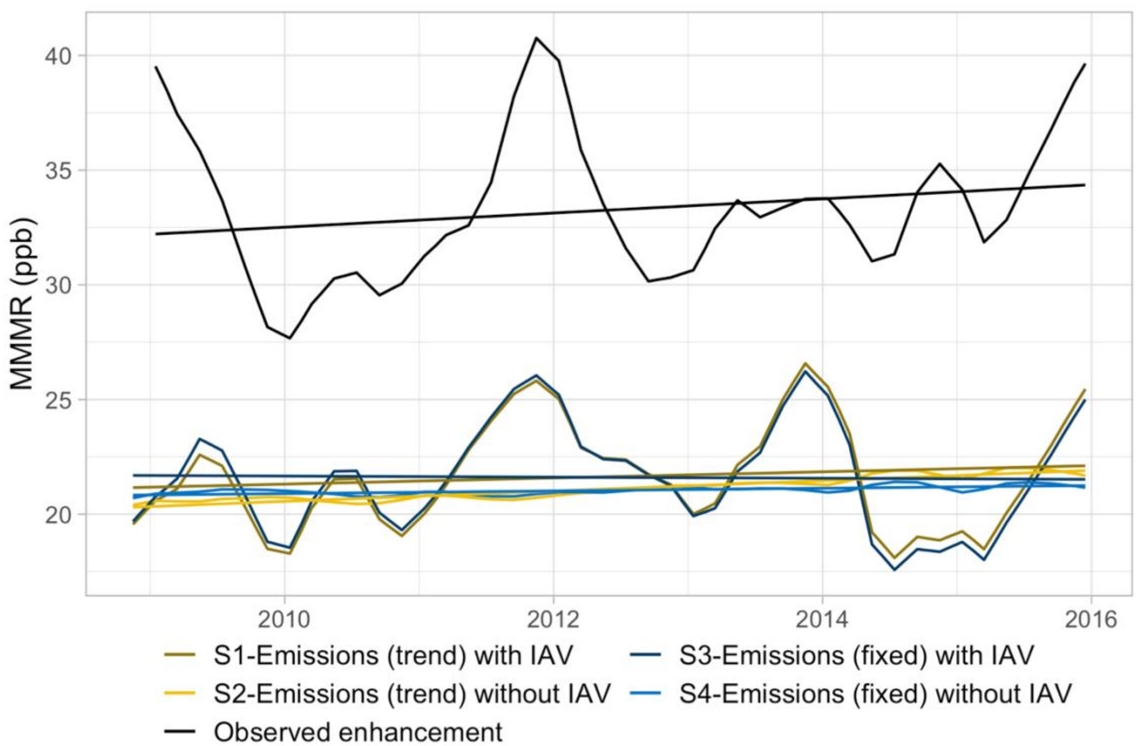

Figure S1. Time series of MMR at site AMT for all 4 modeling scenarios and observed trends

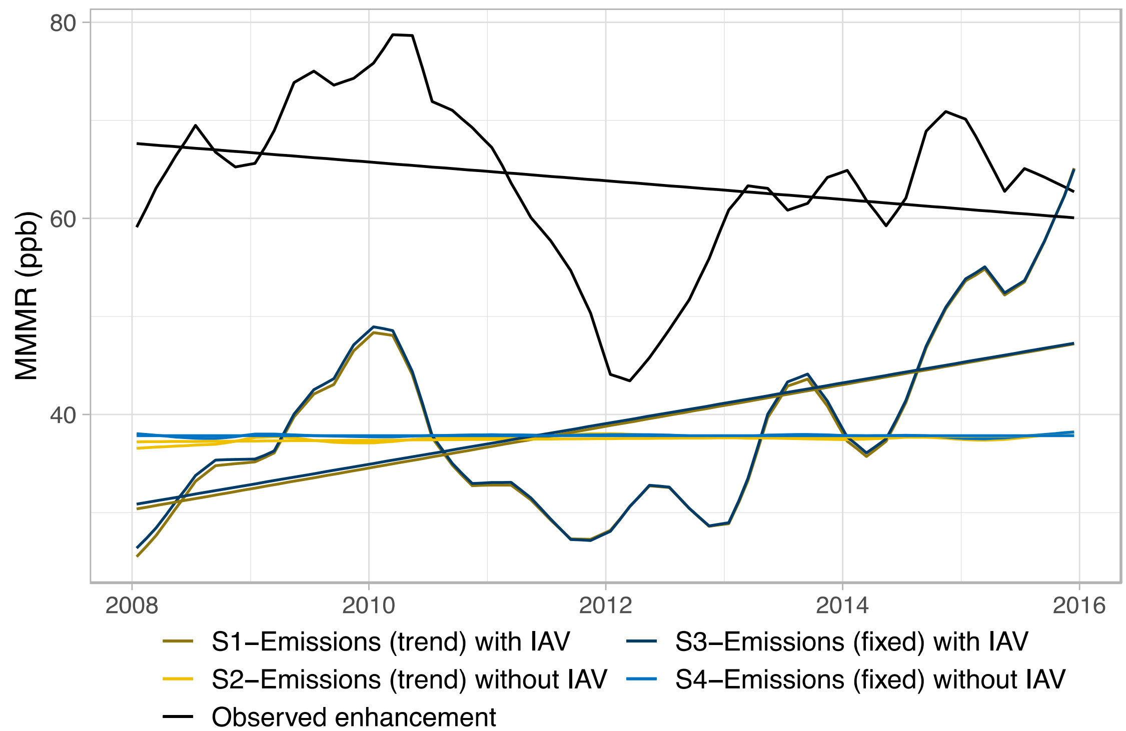

Figure S2. Time series of MMR at site BAO for all 4 modeling scenarios and observed trends

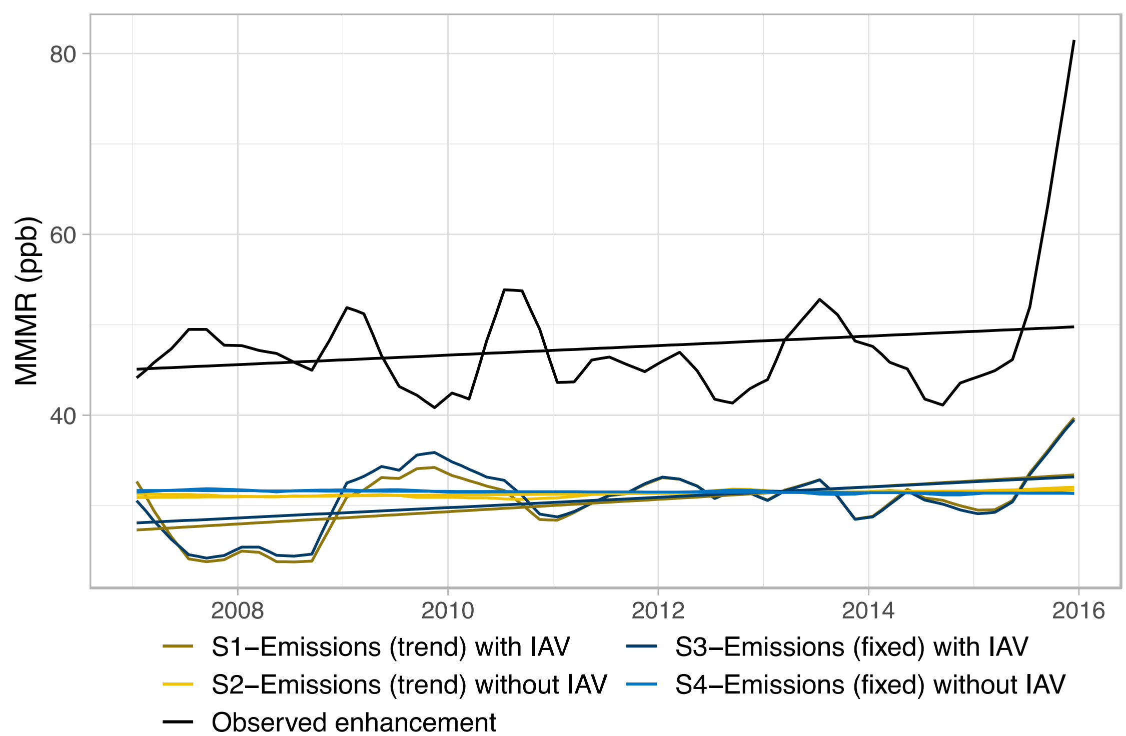

Figure S3. Time series of MMR at site LEF for all 4 modeling scenarios and observed trends

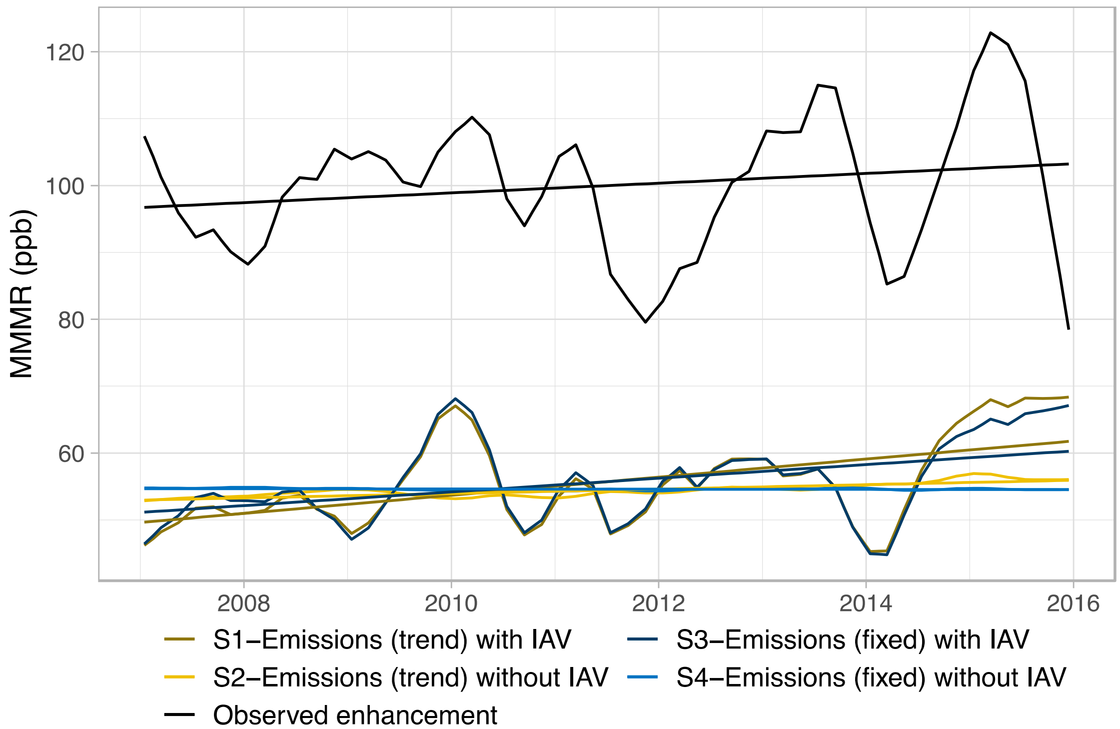

Figure S4. Time series of MMR at site SGP for all 4 modeling scenarios and observed trends

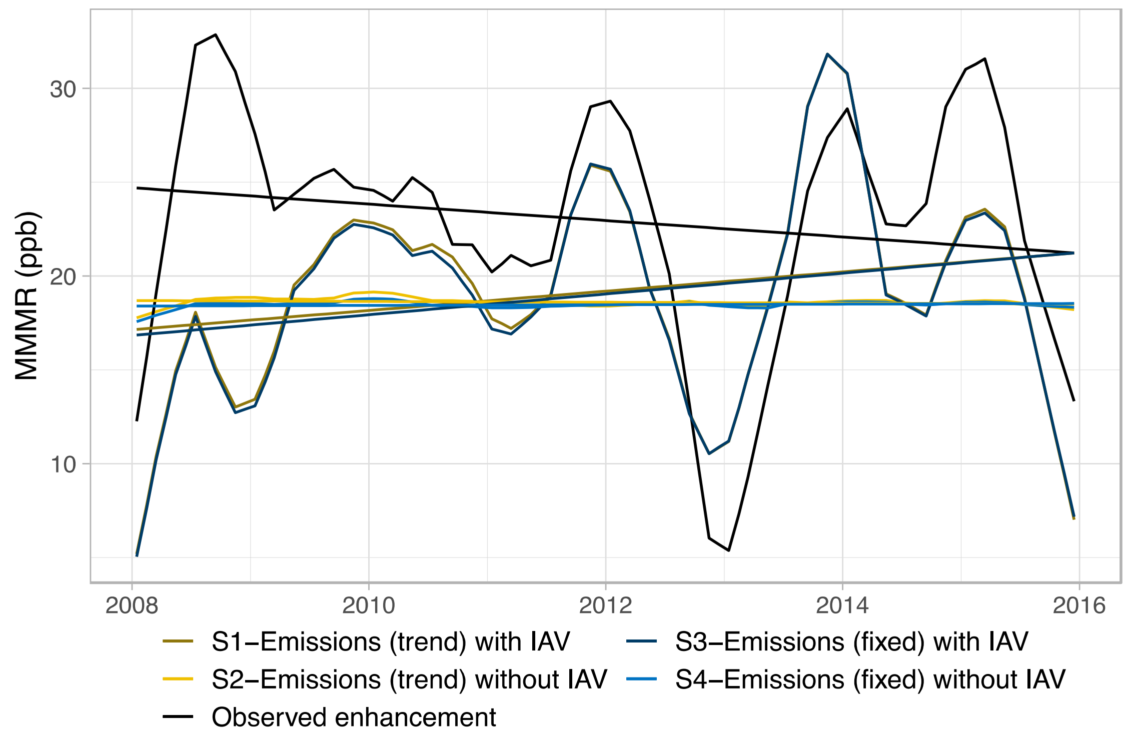

Figure S5. Time series of MMR at site STR for all 4 modeling scenarios and observed trends

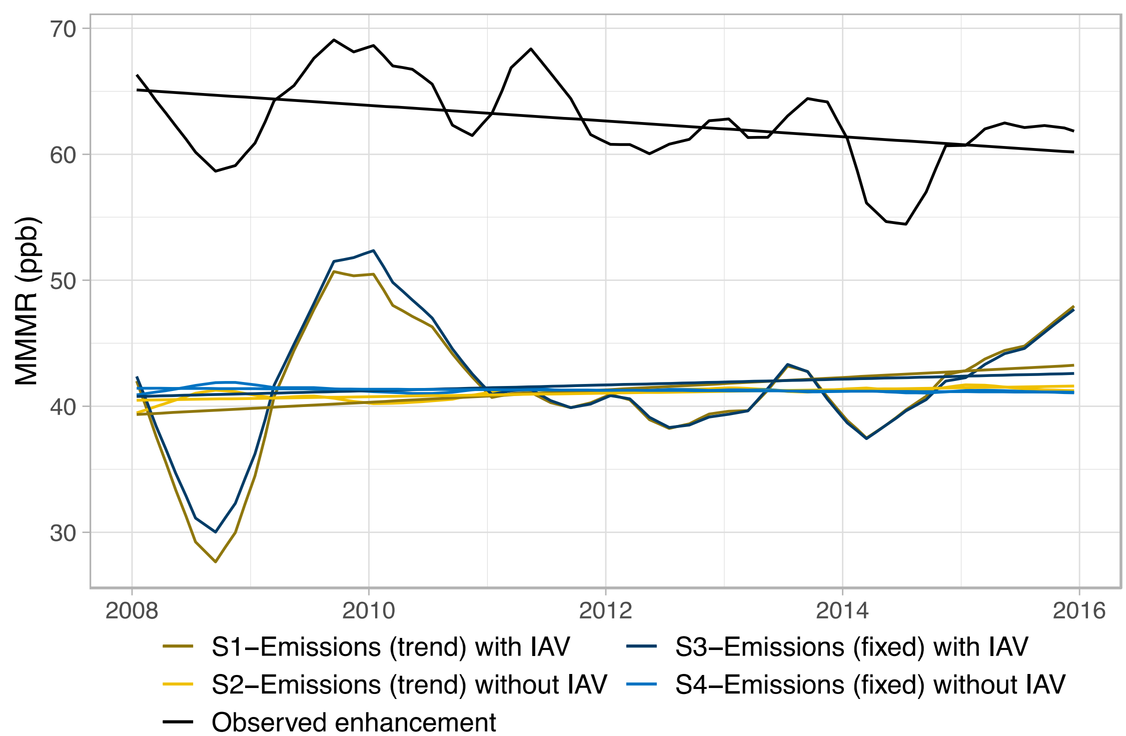

Figure S6. Time series of MMR at site WBI for all 4 modeling scenarios and observed trends

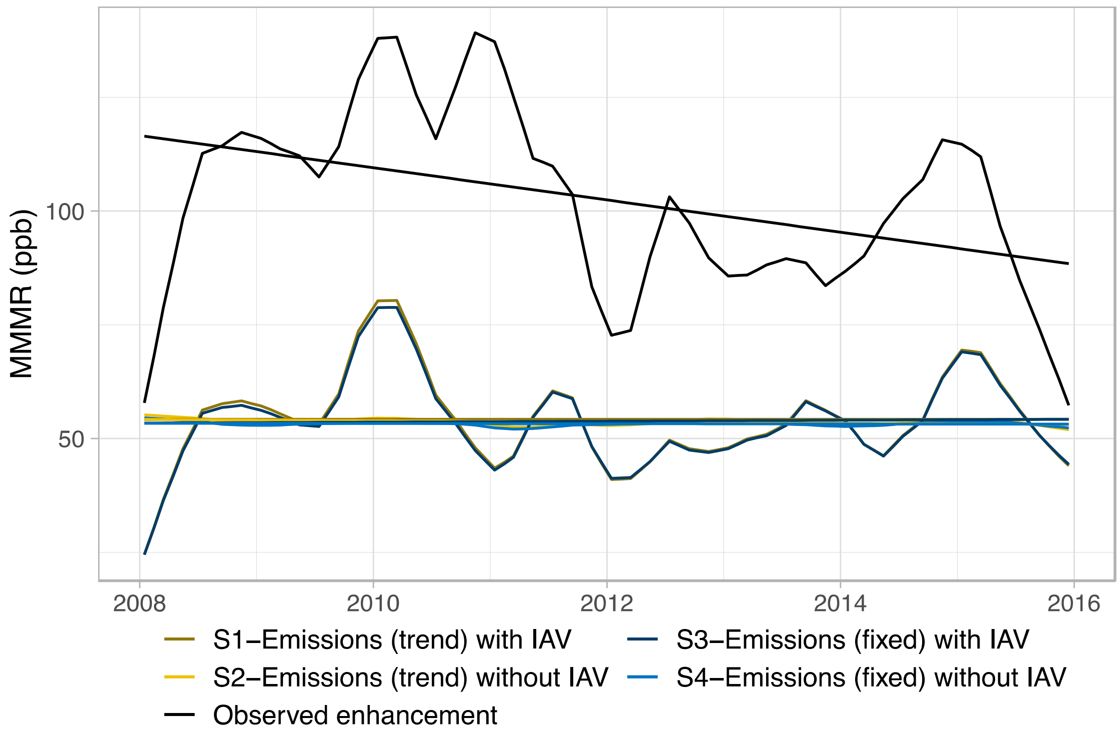

Figure S7. Time series of MMR at site WGC and for all 4 modeling scenarios and observed trends

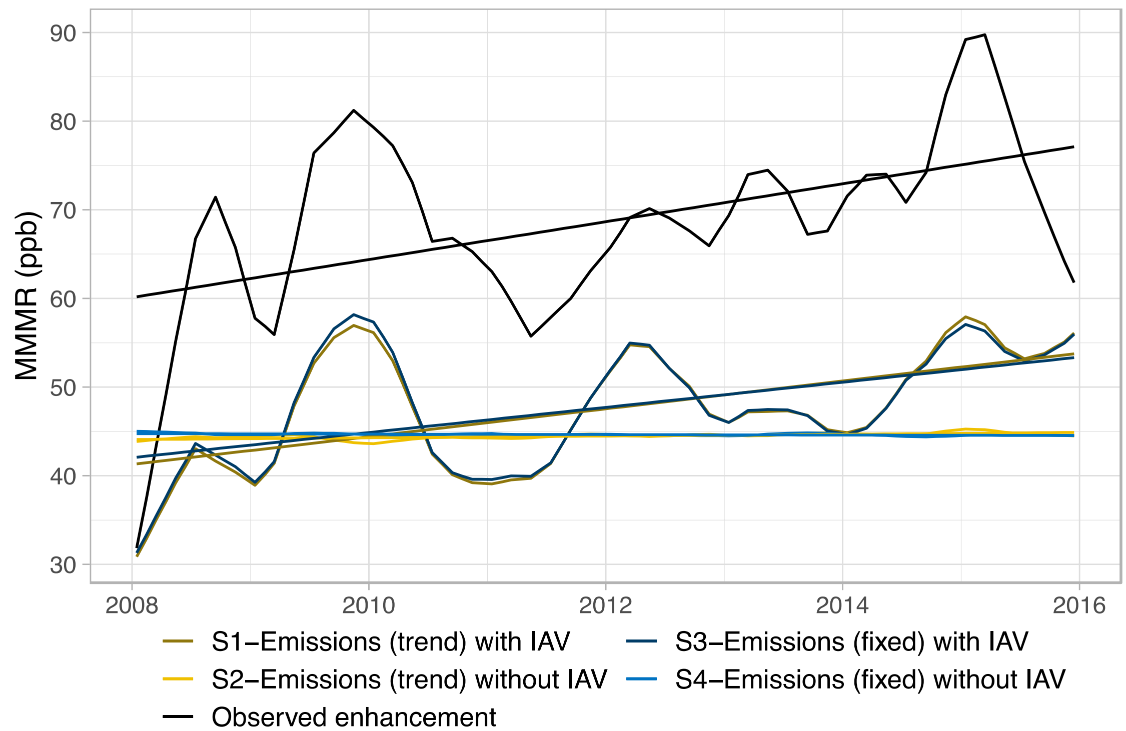

Figure S8. Time series of MMR at site WKT for all 4 modeling scenarios and observed trends

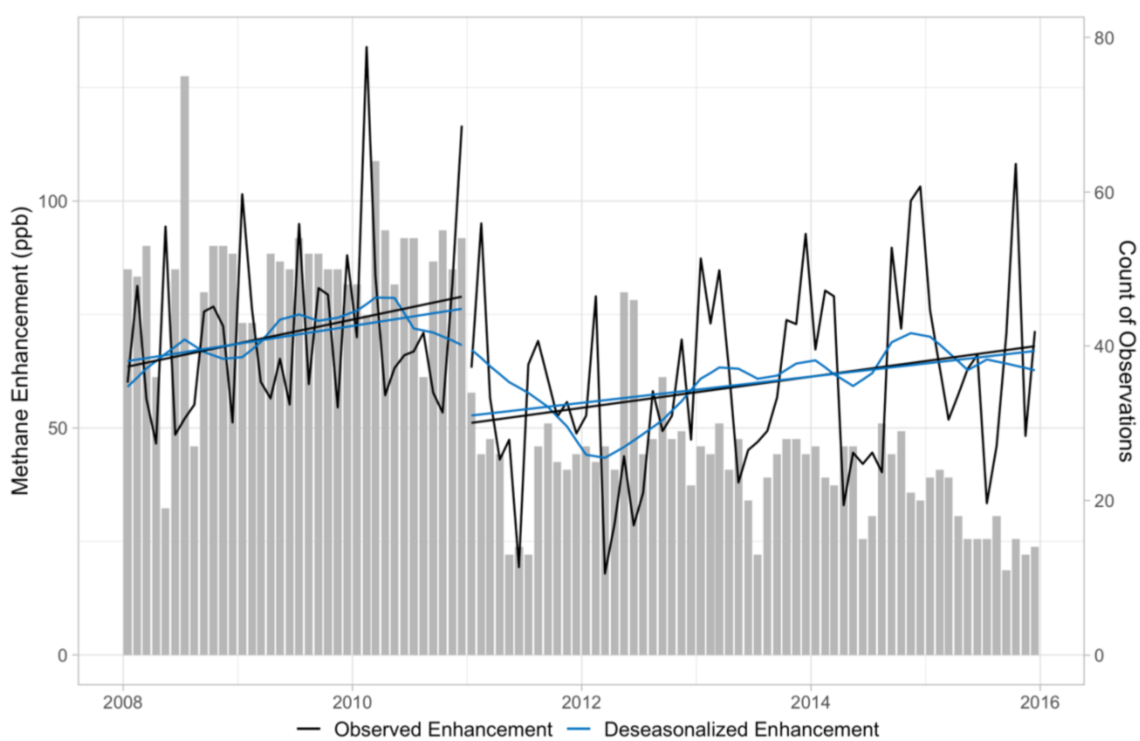

Figure S9. Observed methane enhancement at site BAO with observation frequency

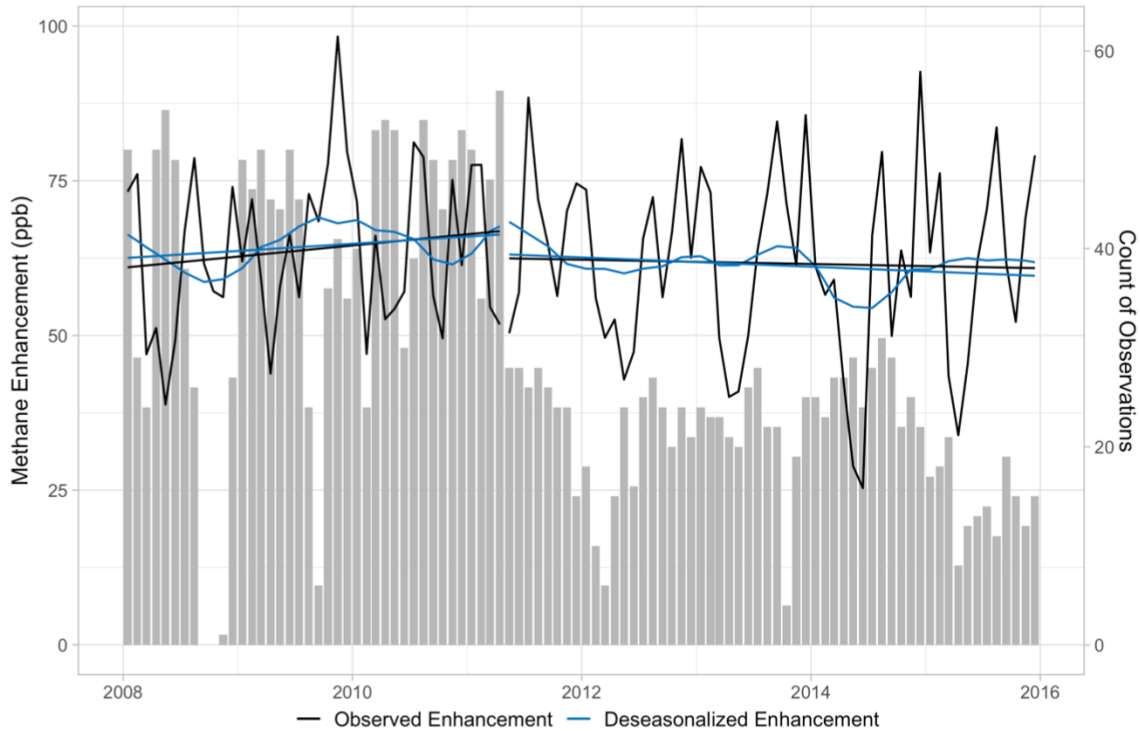

Figure S10. Observed methane enhancement at site WBI with observation frequency

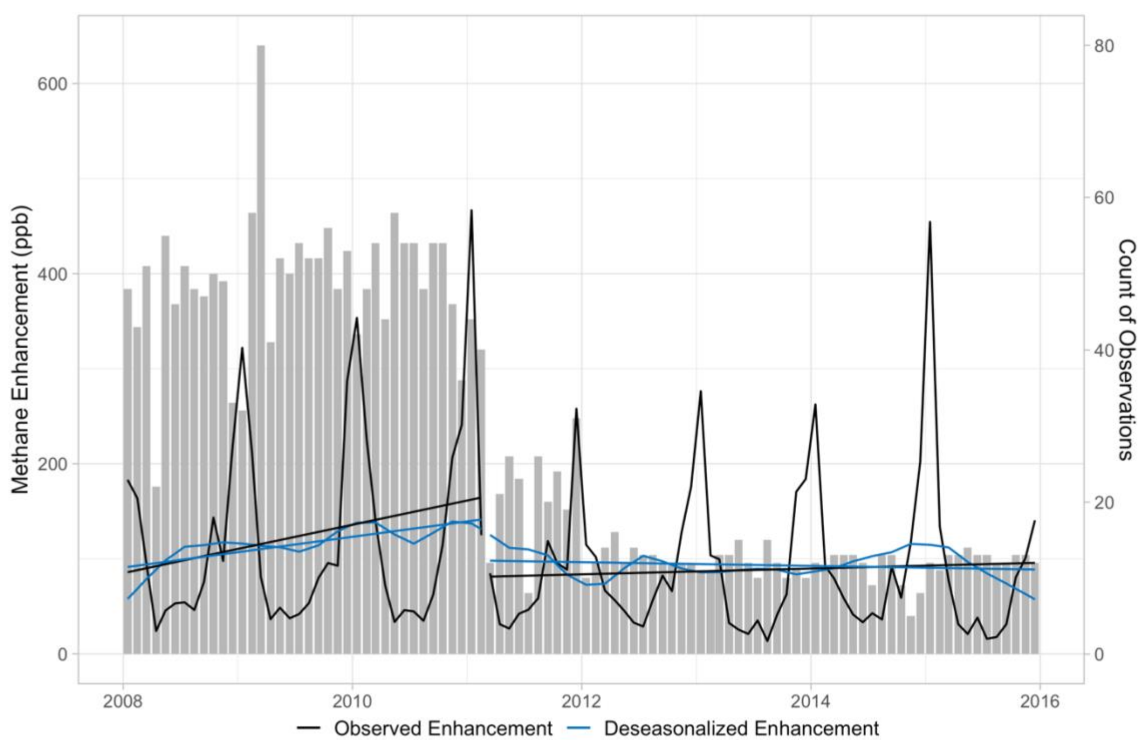

Figure S11. Observed methane enhancement at site WGC with observation frequency

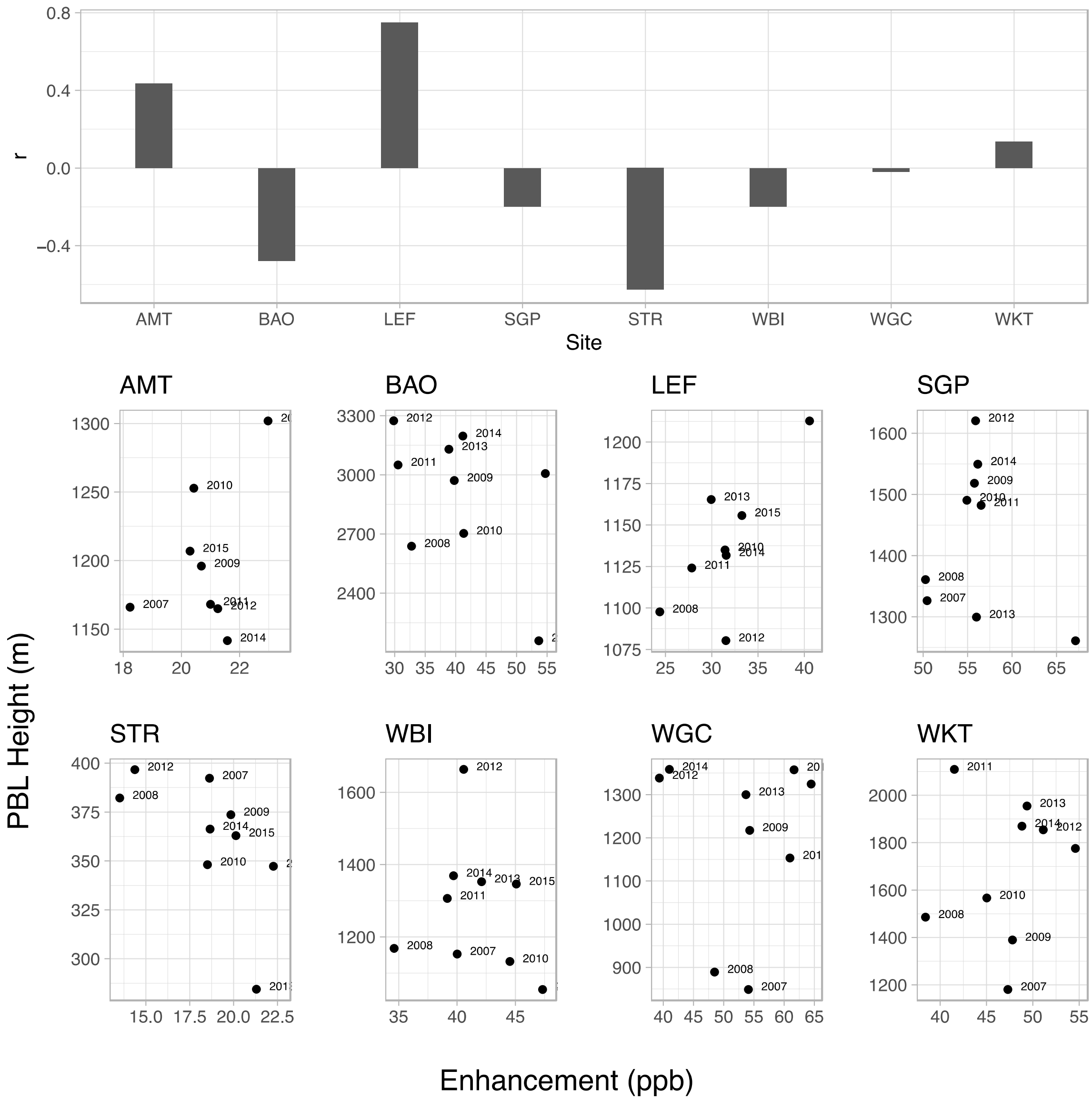

Figure S12. Correlation coefficient between modeled MMR and PBL height parameters for all in-situ monitoring sites.

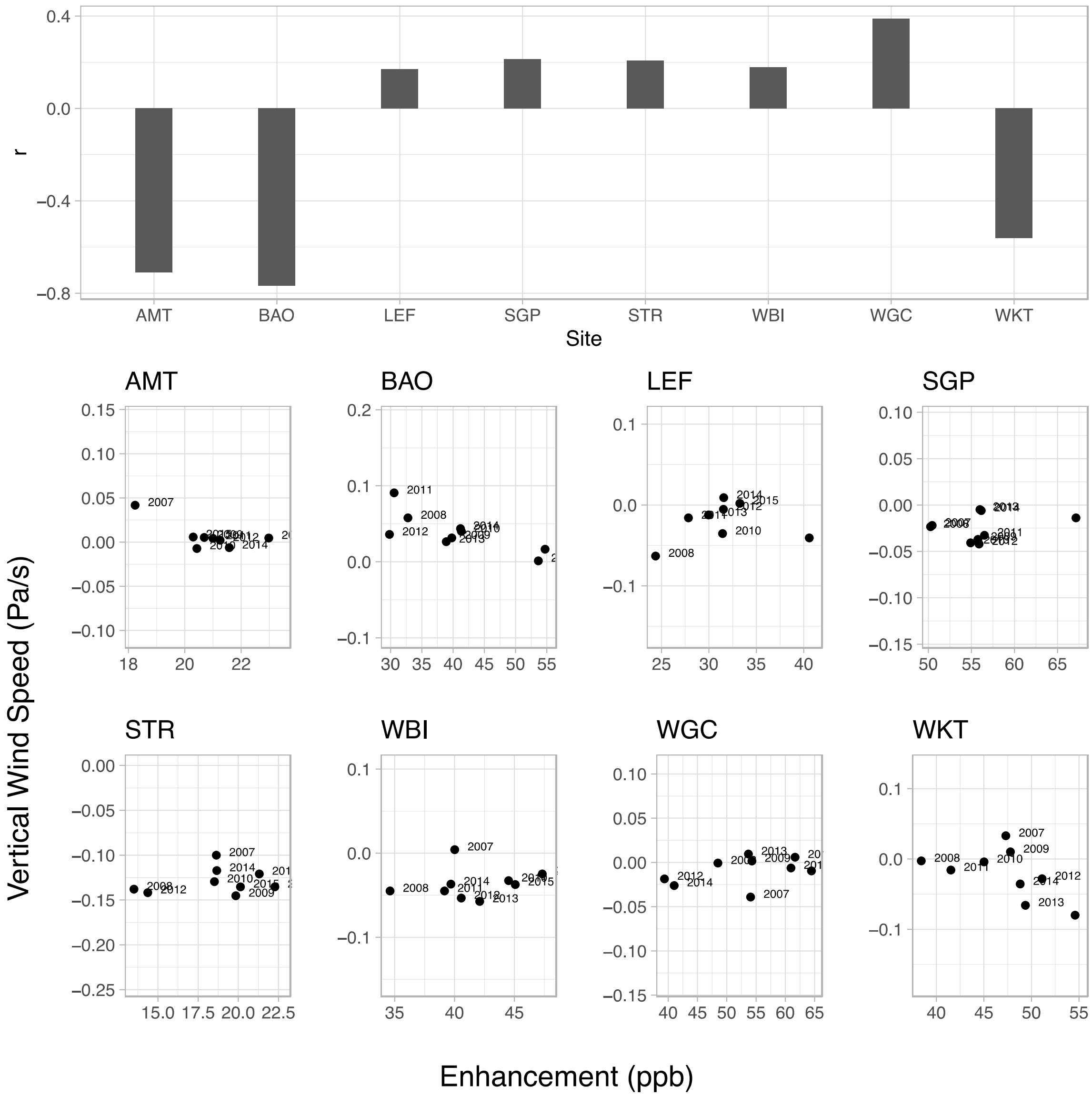

Figure S13. Correlation coefficient between modeled MMR and vertical wind speed for all in-situ monitoring sites.

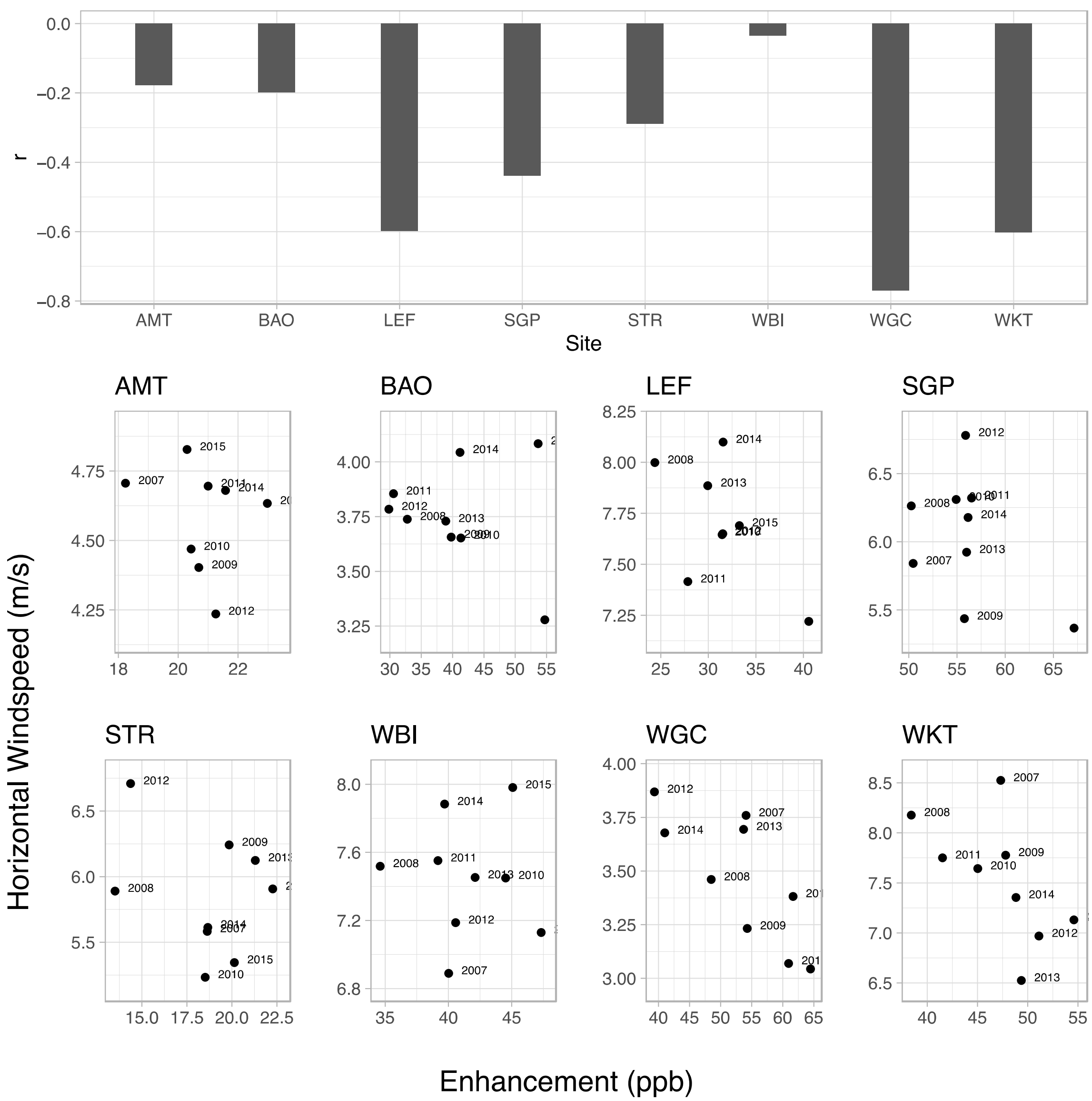

Figure S14. Correlation coefficient between modeled MMR and horizontal windspeed for all in-situ monitoring sites.

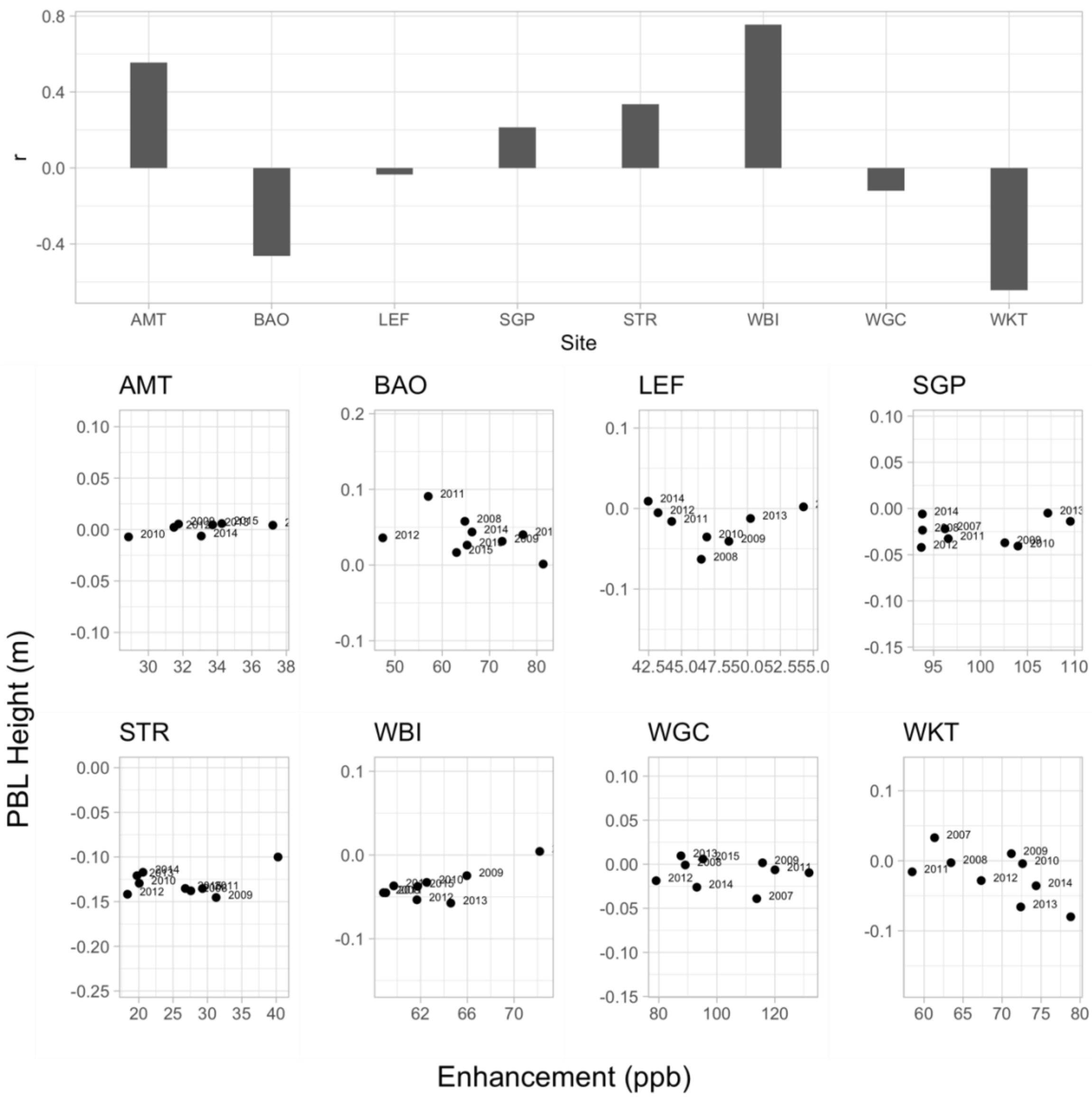

Figure S15. Correlation coefficient between observed MMR and PBL height for all in-situ monitoring sites.

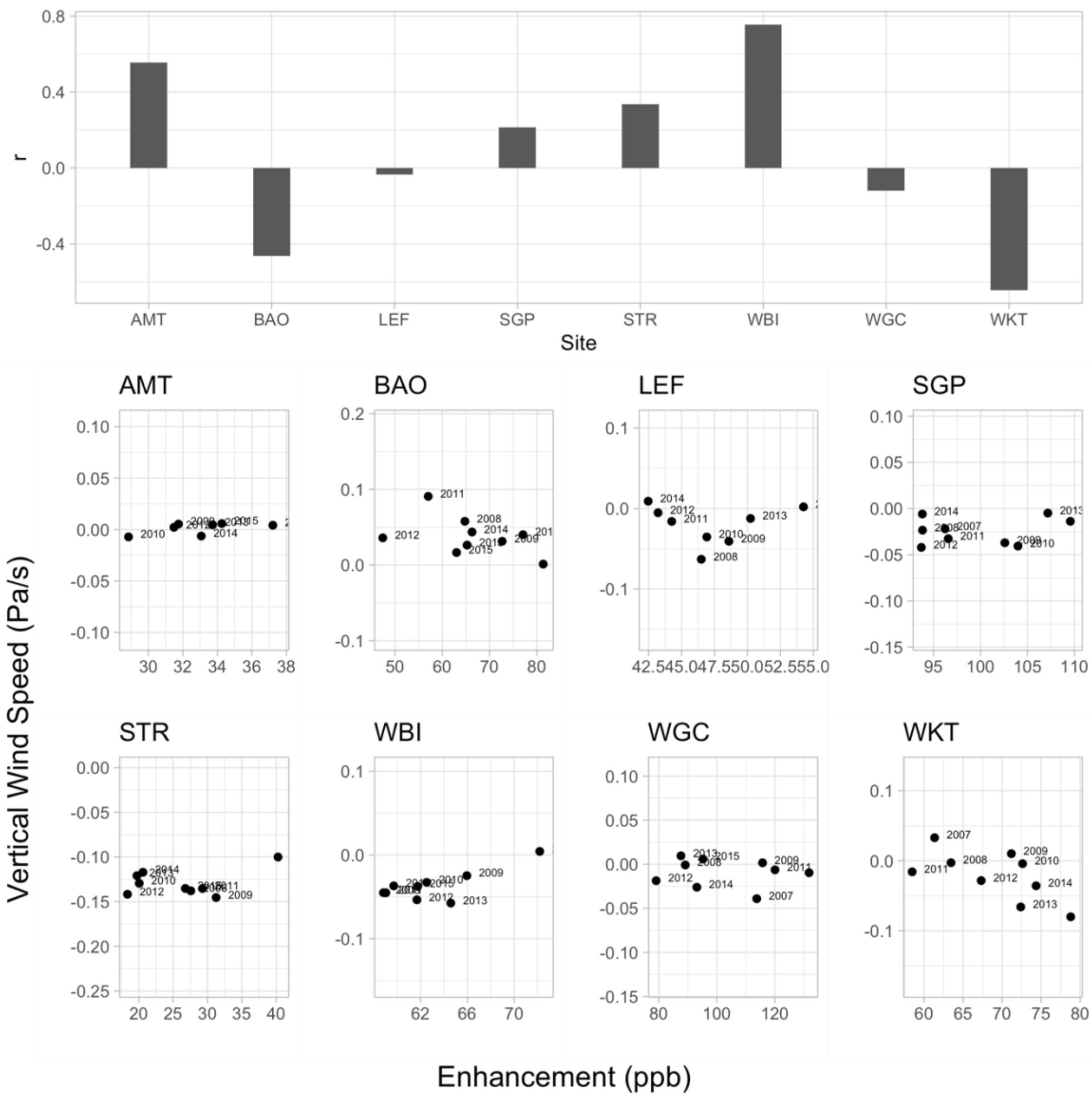

Figure S16. Correlation coefficient between observed MMR and vertical windspeed for all in-situ monitoring sites.

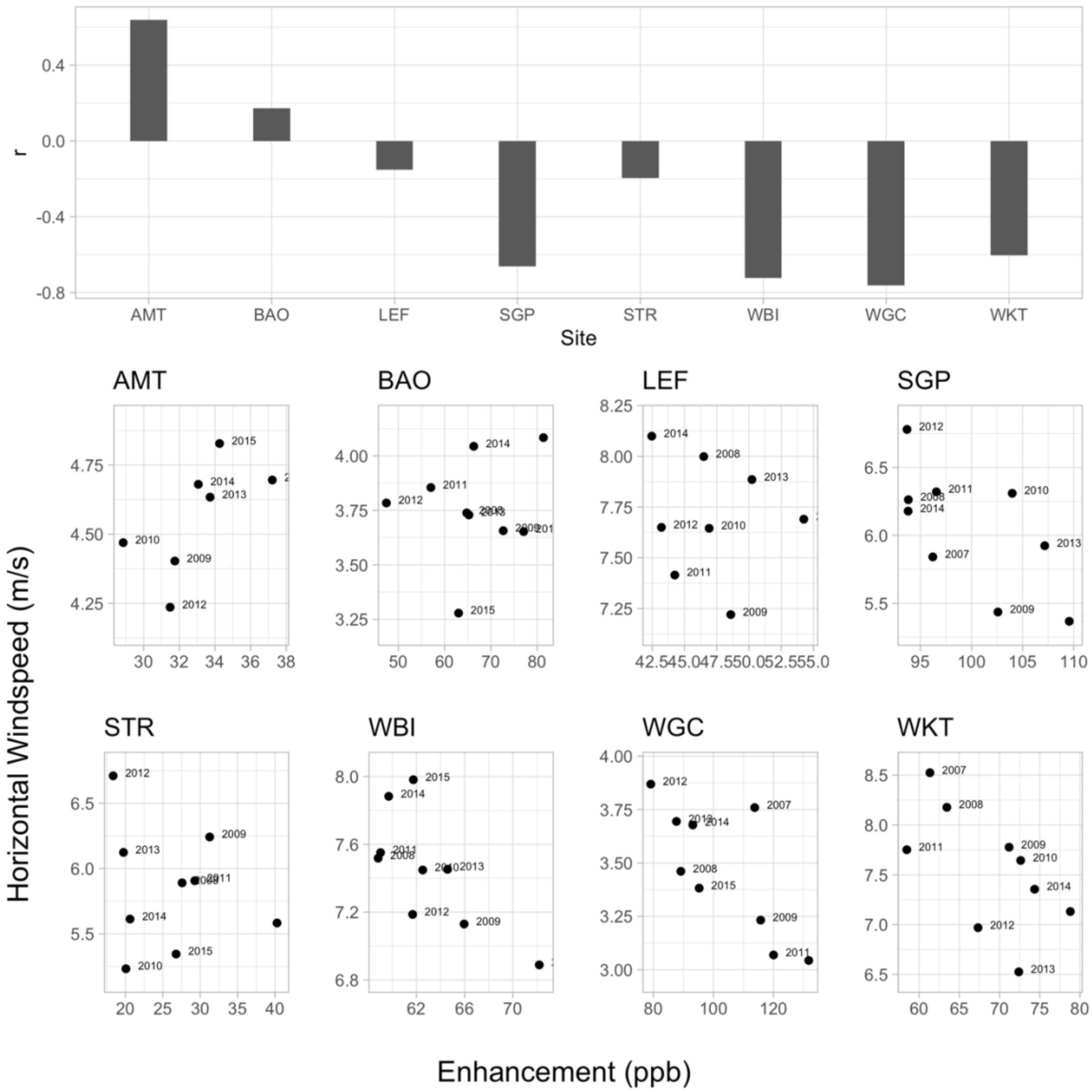

Figure S17. Correlation coefficient between observed MMR and horizontal windspeed for all in-situ monitoring sites.

S3 Additional details on the analysis for GOSAT observations

This section includes supplementary figures describing analysis of the GOSAT observations and the associated model simulations. Figures S18-S21 display the trends in modeled MMR at GOSAT observation locations, averaged into 4° by 4° latitude-longitude grid boxes. These figures display the results for all four of the modeling scenarios, in contrast to Fig. 2 in the main article, which only displays the results for scenario three (no trend in emissions, IAV in meteorology). Figures S18-S21 show that the simulated trend in emissions yields a relatively small change in the model outputs; the trends in MMR for scenario one (trend in emissions, IAV in meteorology) are similar to the trends in MMR estimated for scenario three (no trend in emissions, IAV in meteorology). Similarly, the estimated trends in scenario two (trend in emissions, no IAV in meteorology) are similar to the estimated trends in scenario four (no trend in emissions, no IAV in meteorology). By contrast, the largest difference among simulations (i.e., the largest difference in the estimated trends) is between scenarios that do and do not include IAV in meteorology. Specifically, scenarios one and three, which include IAV in meteorology, are most different from scenarios two and four, which do not include IAV in meteorology. This analysis using GOSAT observations parallels the conclusions of the analysis for the in-situ observation sites; trends in emissions have a modest impact on trends in MMR while IAV in meteorology has a much larger impact.

Figures S22 - S28 further display modeled MMR time series at several prototypical locations (i.e., for several 4° by 4° latitude-longitude grid boxes). These figures provide visualization of the model and observational outputs that are used in trend fitting. Each figure displays annually-averaged MMR for each modeling scenario, and trend lines fitted to each of these model time series. These figures further reinforce the large differences between model simulations that do and do not include IAV in meteorology (e.g., scenarios one and three versus two and four).

Note that we also subtract a methane background or boundary condition from the GOSAT observations before plotting the time series in Figures S22 - S28 and before fitting a trendline, as in Fig. 2. By subtracting a background or boundary condition, we remove global methane trends from the analysis and focus only on trends over North America. We construct this methane background using the same approach as in Sheng et al. (2018). Specifically, within each year and each 4° by 4° grid box, we identify the GOSAT observations with the lowest observed mixing ratios (the lowest 5th percentile). We then average those observations in the lowest 5th percentile and use this average as the methane background for that year in that grid box. Sheng et al. (2018) used this approach to calculating the background because multiple existing studies have used similar percentile approaches for estimating regional backgrounds (e.g., Goldstein et al. 1995).

The approach used to estimate the background for GOSAT observations is not the same as the approach used for in situ observations in this study (Sect. S1). We do so for multiple reasons. First, we want to directly compare against existing studies of methane emissions from North America and have therefore used the same approach for GOSAT and in situ observations, respectively, as in existing studies (e.g., Jeong et al. 2013, Miller et al. 2013, and Sheng et al. 2018). Second, there is always a possibility that GOSAT observations may exhibit biases relative to in situ observations. We therefore use GOSAT observations to build the background for the GOSAT analysis and in situ observations to build the background for the in-situ analysis. This approach ensures that any discrepancies between in situ and satellite observations do not contaminate the estimated background.

The final set of figures associated with this section of the supplement provides more in-depth visualization of the relationship between MMR and the magnitude of the local footprint (Fig. S29-S35). In the main article, we argue that local meteorological processes are likely driving IAV in MMR at the GOSAT observation sites. We argue this point in the main article by exploring correlations between MMR and the annually-averaged magnitude of the local footprint (Fig. 3). Note that we define the local footprint as a 4° latitude/longitude radius area around the observation location. Figures S29-S35 show scatter plots comparing MMR and the magnitude of the local footprint for several prototypical locations. In Fig. 3, we find that MMR and the magnitude of the local footprint are closely correlated at most locations. The scatterplots shown here further confirm that point.

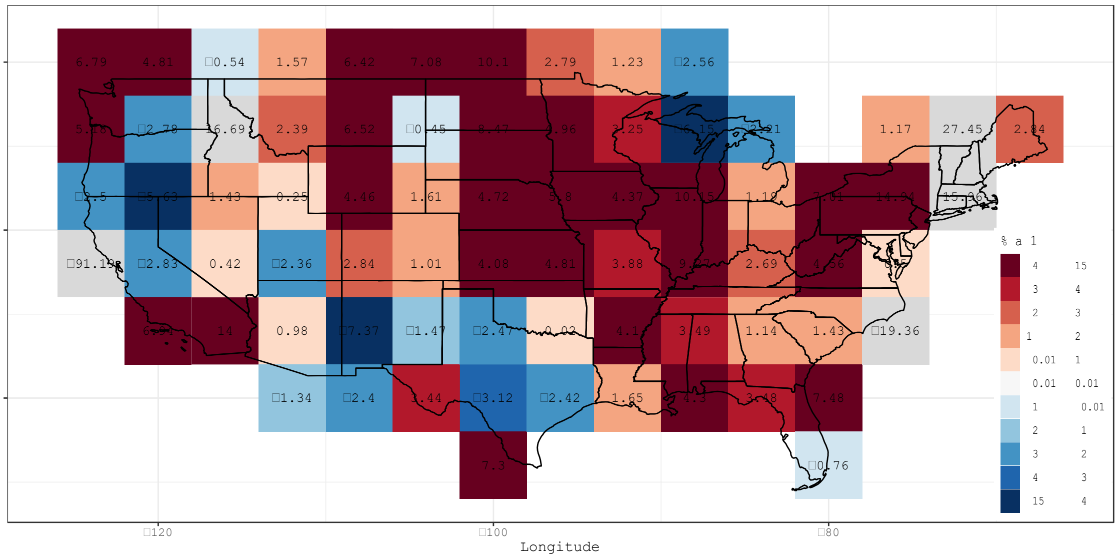

Figure S18. Modeled MMR trends using GOSAT observations for scenario 1

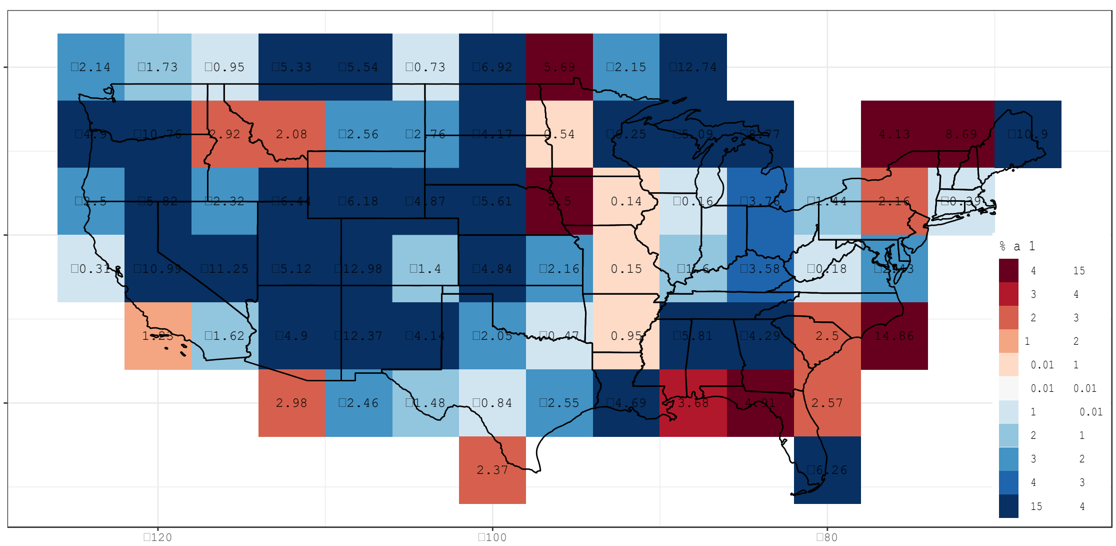

Figure S19. Modeled MMR trends using GOSAT observations for scenario 2

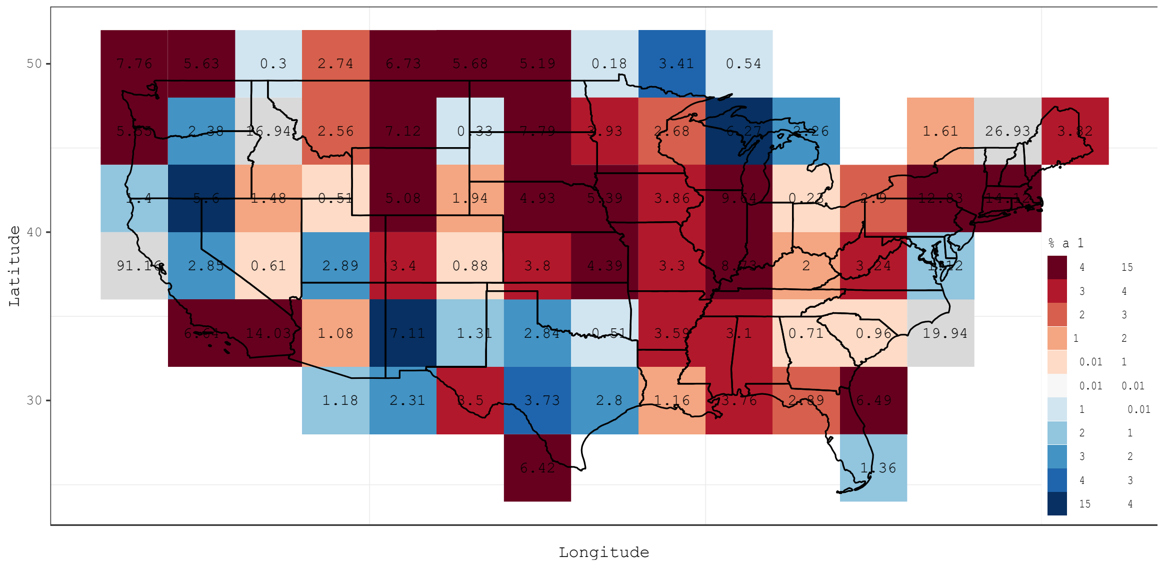

Figure **S20.** Modeled MMR trends using GOSAT observations for scenario 3

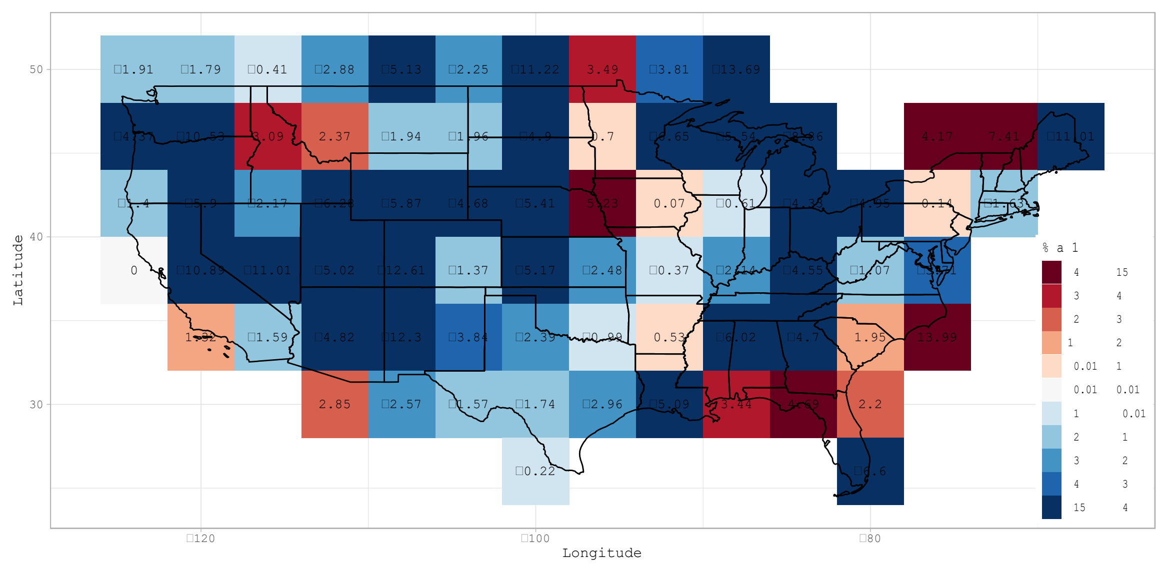

Figure S21. Modeled MMR trends using GOSAT observations for scenario 4

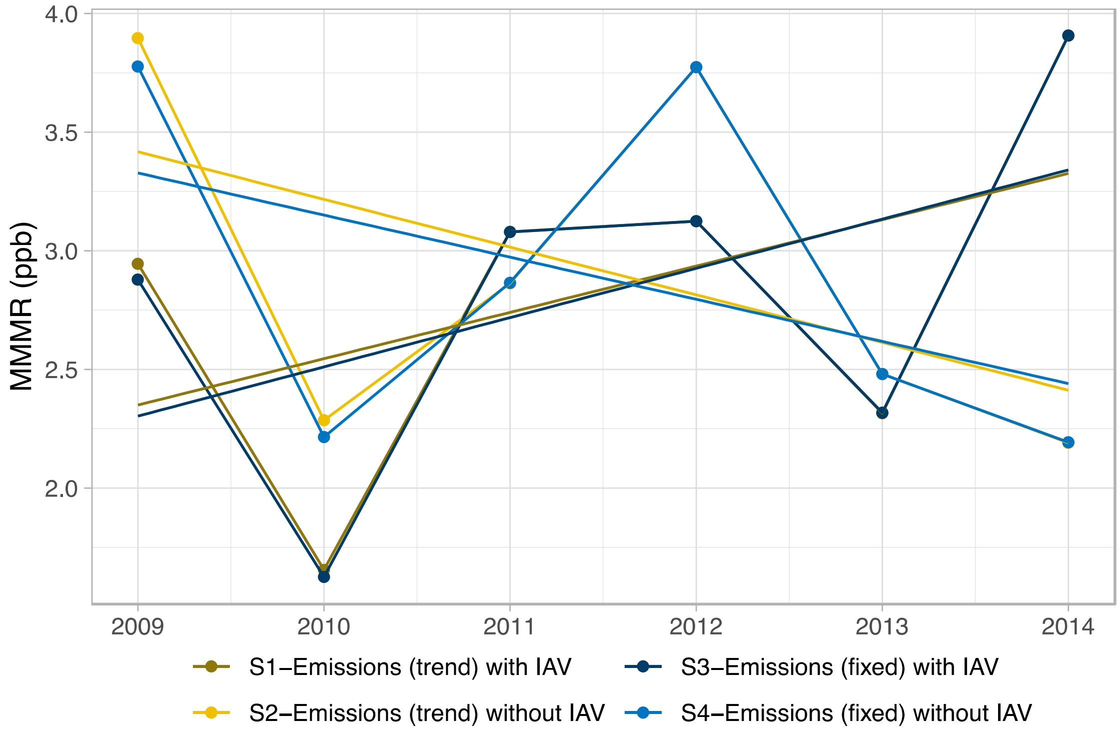

Figure S22. Time series of MMR for GOSAT prototypical location 1 (West Washington State)

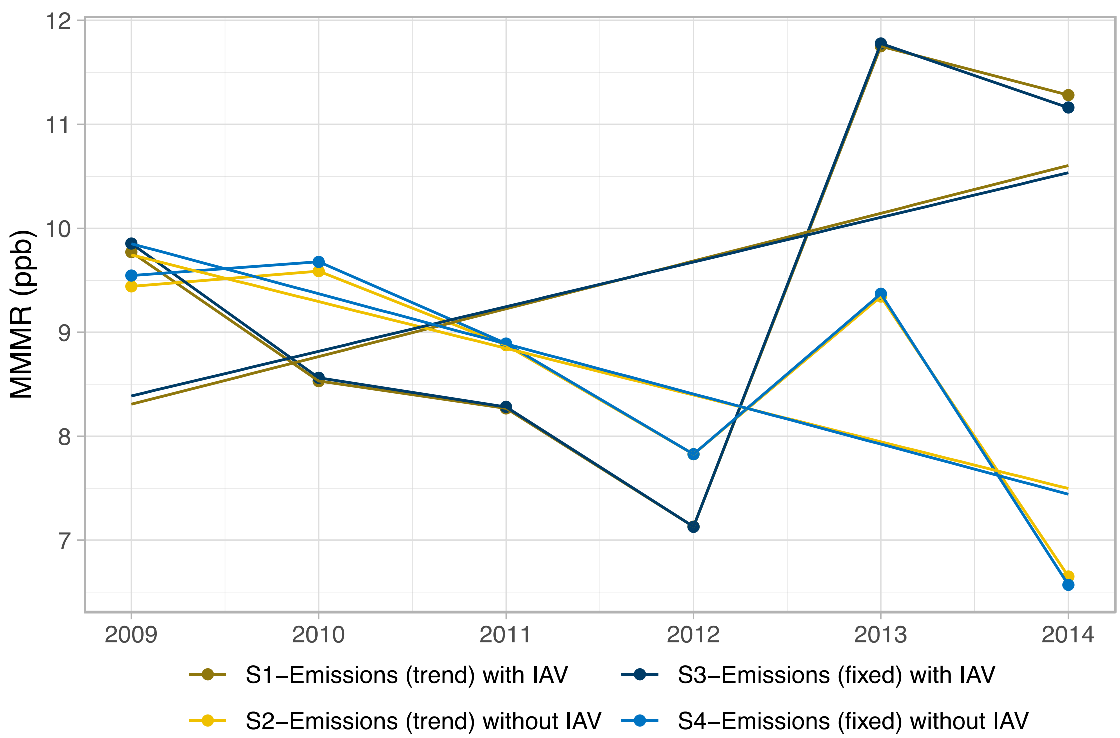

Figure S23. Time series of MMR for GOSAT prototypical location 2 (West Kansas)

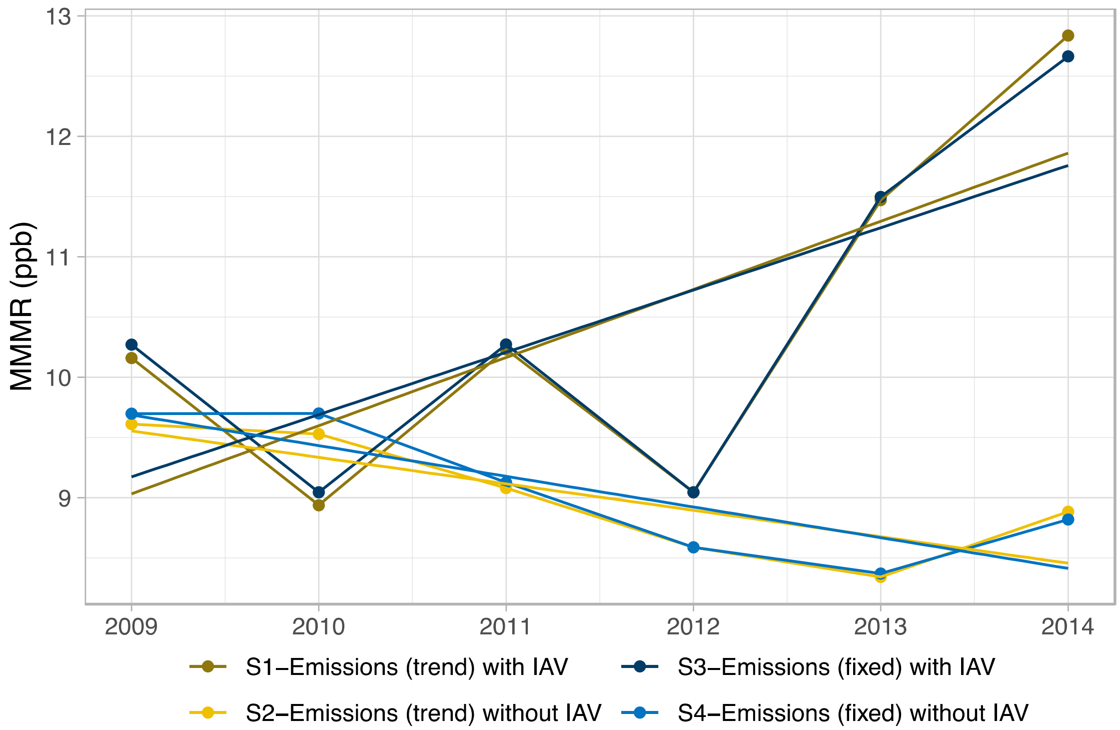

Figure S24. Time series of MMR for GOSAT prototypical location 3 (East Kansas)

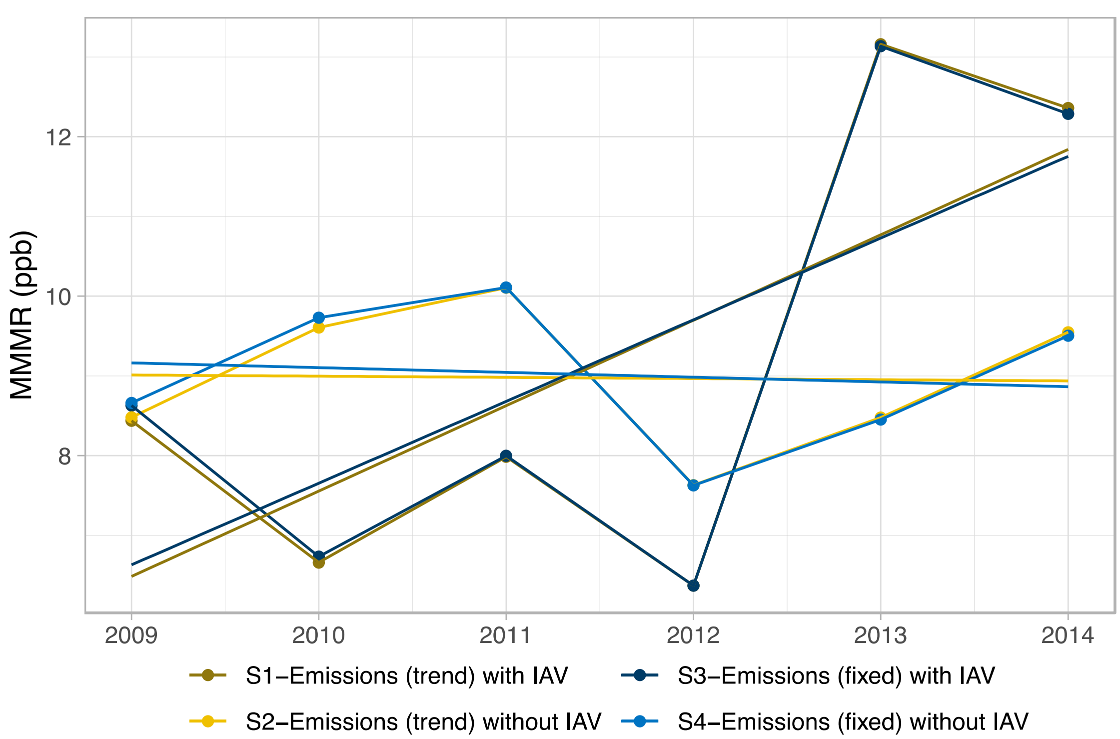

Figure S25. Time series of MMR for GOSAT prototypical location 4 (Chicago area)

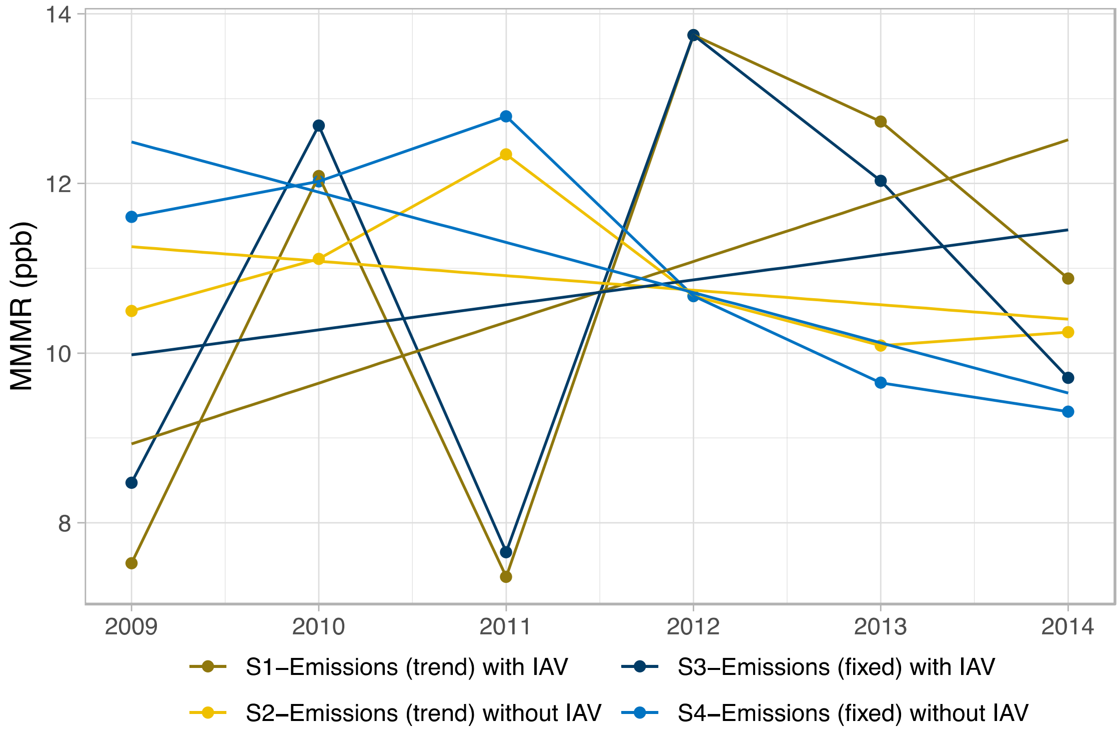

Figure S26. Time series of MMR for GOSAT prototypical location 5 (West New York - West Pennsylvania)

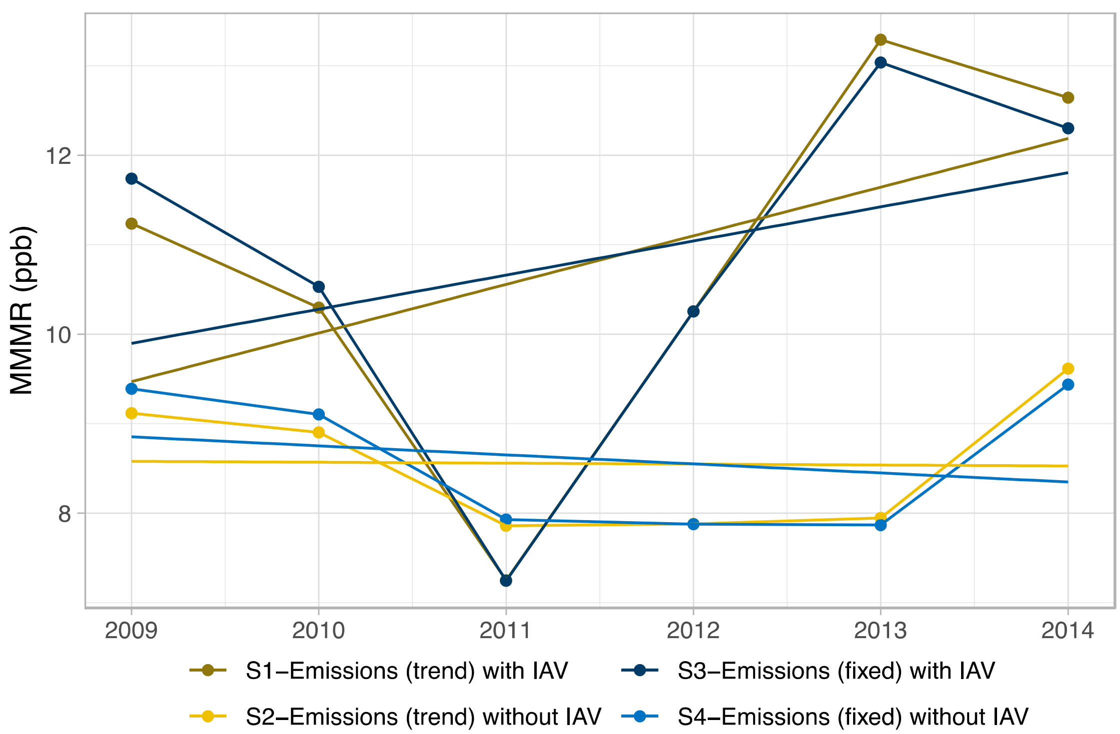

Figure S27. Time series of MMR for GOSAT prototypical location 6 (West Virginia - Southwest Virginia)

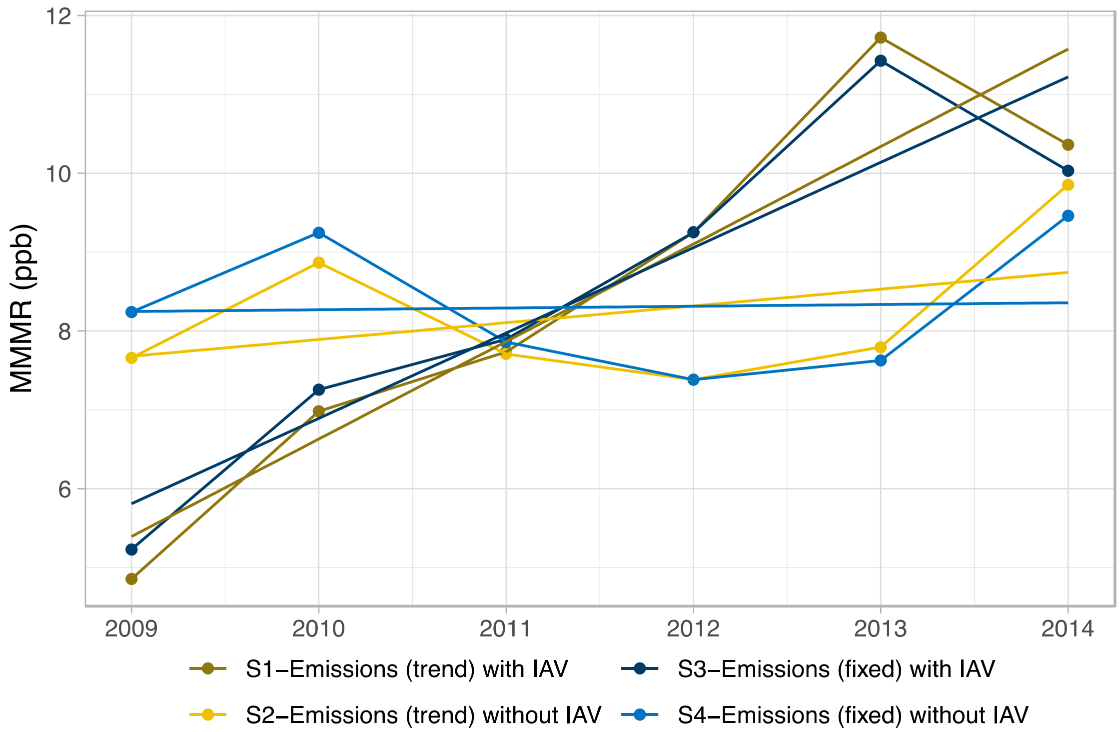

Figure S28. Time series of MMR for GOSAT prototypical location 7 (East New York - East Pennsylvania)

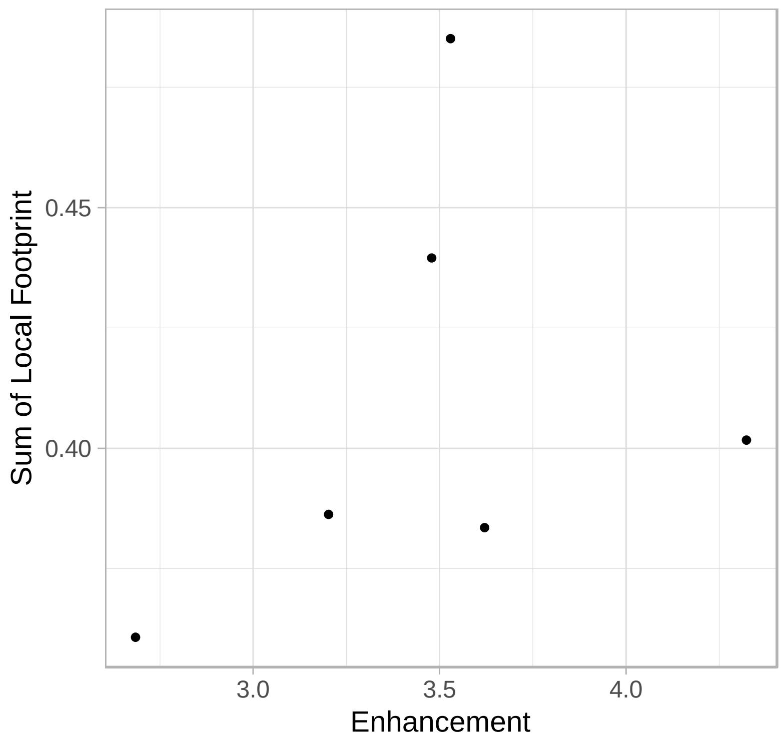

Figure S29. Scatter plot of total modeled enhancement vs. local footprints for GOSAT prototypical location 1 (West Washington State)

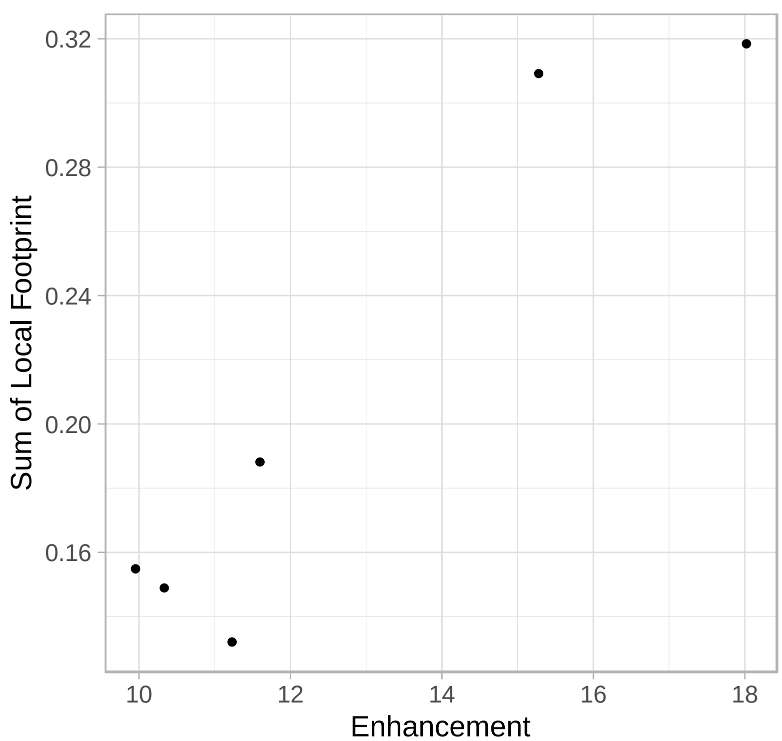

Figure S30. Scatter plot of total modeled enhancement vs. local footprints for GOSAT prototypical location 2 (West Kansas)

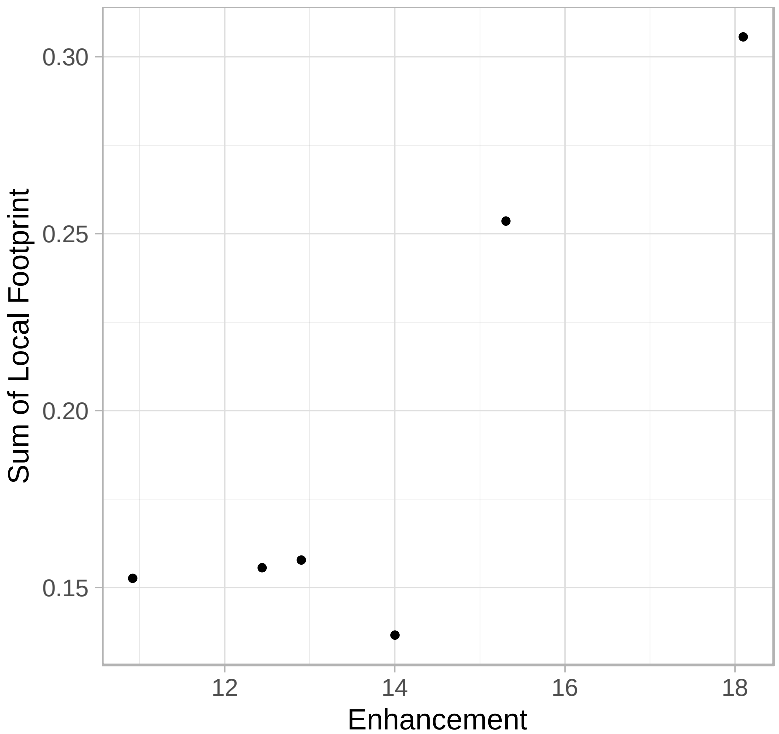

Figure S31. Scatter plot of total modeled enhancement vs. local footprints for GOSAT prototypical location 3 (East Kansas)

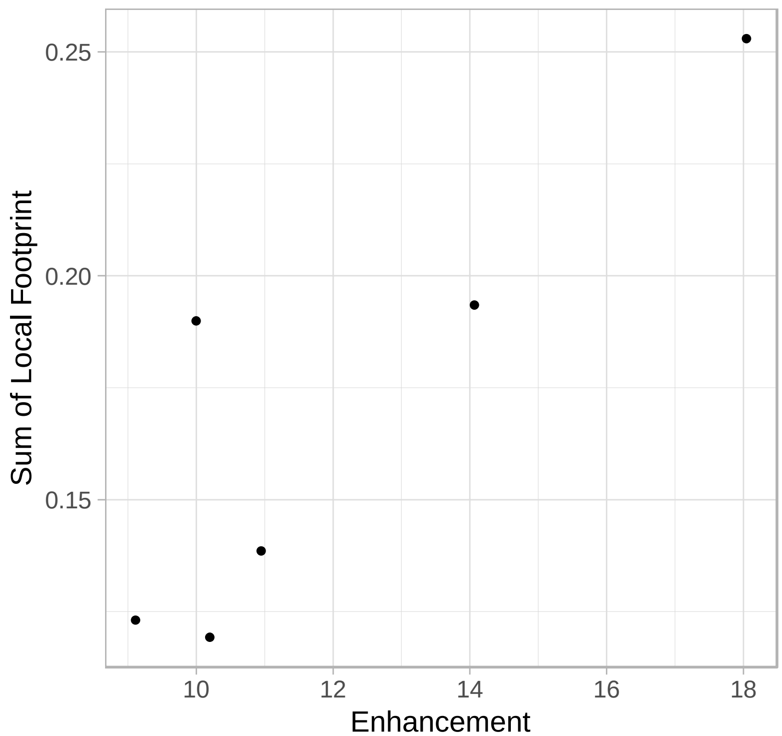

Figure S32. Scatter plot of total modeled enhancement vs. local footprints for GOSAT prototypical location 4 (Chicago area)

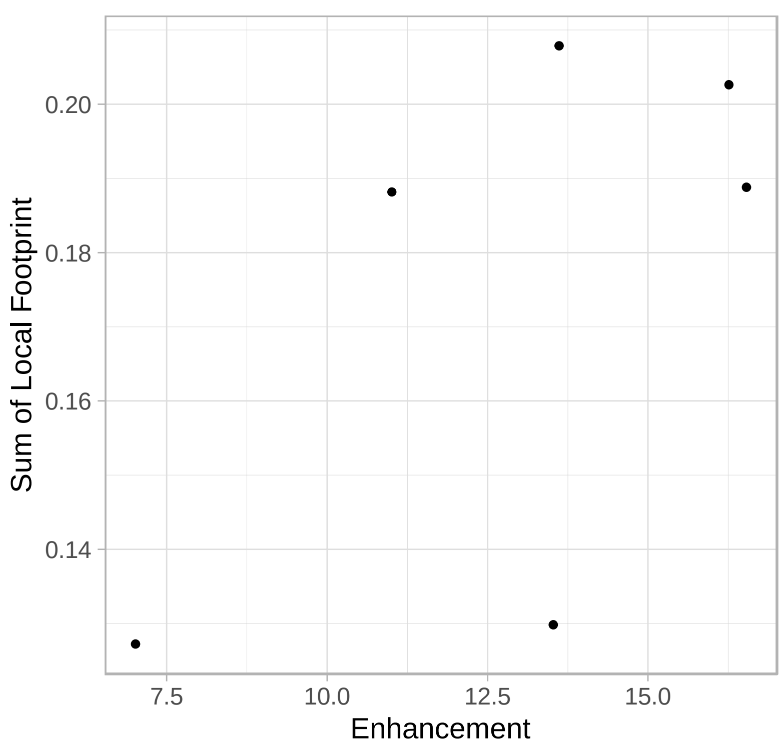

Figure S33. Scatter plot of total modeled enhancement vs. local footprints for GOSAT prototypical location 5 (West New York - West Pennsylvania)

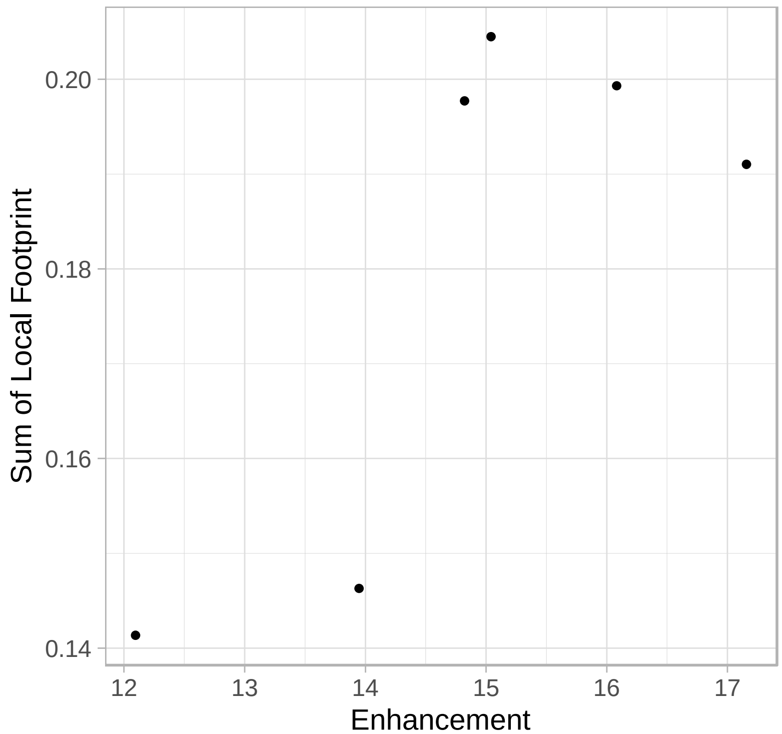

Figure S34. Scatter plot of total modeled enhancement vs. local footprints for GOSAT prototypical location 6 (West Virginia - Southwest Virginia)

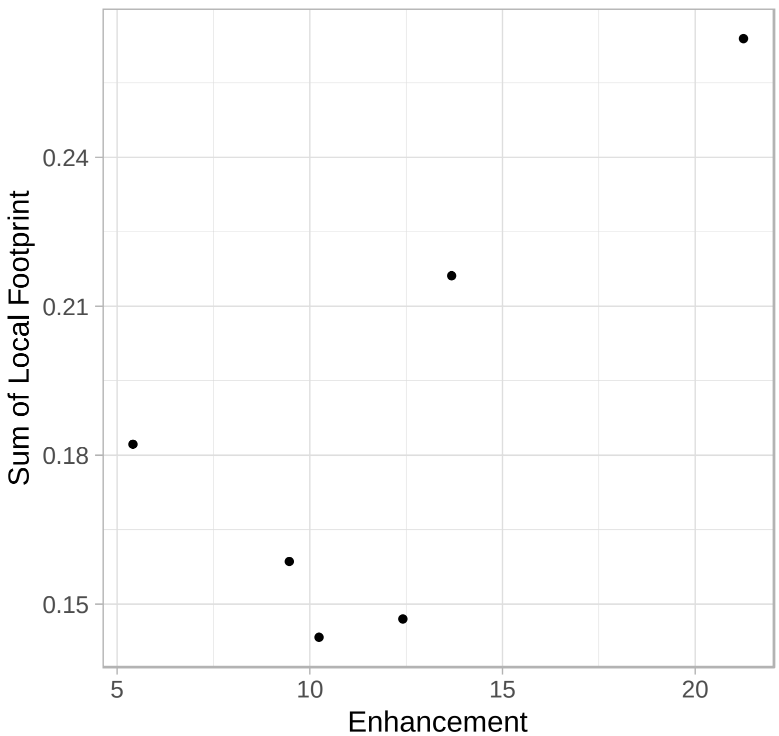

Figure S35. Scatter plot of total modeled enhancement vs. local footprints for GOSAT prototypical location 7 (East New York - East Pennsylvania)

S4 Sensitivity simulations

We conduct two sensitivity tests at sites in oil and gas producing regions (SGP and WKT) to (1) evaluate the sensitivity of the STILT model outputs to the meteorological product used, and (2) investigate possible effects of gaps or irregularities in atmospheric sampling.

For the first sensitivity study, we generate a second set of STILT simulations using meteorology from North American Mesoscale Forecast System 12 km (NAM-12) (NCEP, 2015). We use NAM-12 as an alternative meteorology product in the sensitivity simulation because this product has been used in several existing regional GHG modeling studies (Huang et al. 2019; Ren et al. 2018; Sargent et al. 2021). This product also has a relatively fine spatial resolution (12 km) relative to some other meteorological products, making it a good choice for regional-scale GHG modeling. Figures S32a and S33a show the model simulations using NAM-12. Both figures show the monthly-average MMR (i.e., no methane background or boundary condition added; not de-seasonalized). This setup for Figs. S32-33 allows for a direct visual comparison among the different sets of model outputs.

In both the NAM-12 STILT (Fig. S35a and S36a) and WRF-STILT (Fig. S35c and S36c) simulations, a trend in emissions has a small impact on the overall modeled timeseries. For example, the differences between S1 and S3 are small relative to overall variability in

MMR across both sets of model results. By contrast, we do find that the two models sometimes yield different MMR estimates for individual months. For example, NAM-12 tends to estimate higher peak MMR values relative to WRF simulations. Despite these differences between models, the overall impact of a trend in emissions is similar relative to the overall variability in each timeseries.

We further conduct a sensitivity test to evaluate the possible impacts of irregular sampling on the modeled timeseries. In general, flask samples are collected in the afternoons at each tower site, but there is some variability and gaps in sampling frequency. For example, there are typically 30-40 flasks available per month at WKT in years 2008-2010, but sampling frequency drops to ~10 observations per month in years 2012-2015. There are also individual months with relatively few samples, including September, 2008, which had about a quarter as many observations at WKT compared to surrounding months. In contrast to WKT, SGP consistently has been 4-5 observations per month during the study period.

In this sensitivity test, we compute NAM-12 STILT footprints for 1pm local time each day and construct modeled timeseries based on this output (Figs. S35b and S36b). The timeseries at WKT look nearly identical to one another; the model simulations with a fixed, daily sampling time look very similar to the modeled timeseries using the actual observed sampling times (Figs. S36a-b). By contrast, the simulations at SGP show noticeable differences compared to the timeseries using observed sampling times (Figs. S35a-b). We suspect that the low sampling frequency at SGP yields a monthly-averaged timeseries with high variability; the small number of samples collected each month means that the monthly average can vary greatly from one month to another. By contrast, the timeseries in the fixed experiments displays much less month-to-month variability, likely because there are more model points in each month to average over.

Overall, we conclude that sampling frequency and regularity can have an impact on MMR, particularly when those timeseries are averaged to aggregate timescales (e.g., monthly). With that said, the impact of a trend in emissions is small in all cases relative to overall monthly variability in MMR (e.g., S1 versus S3 in Figs. S35-36).

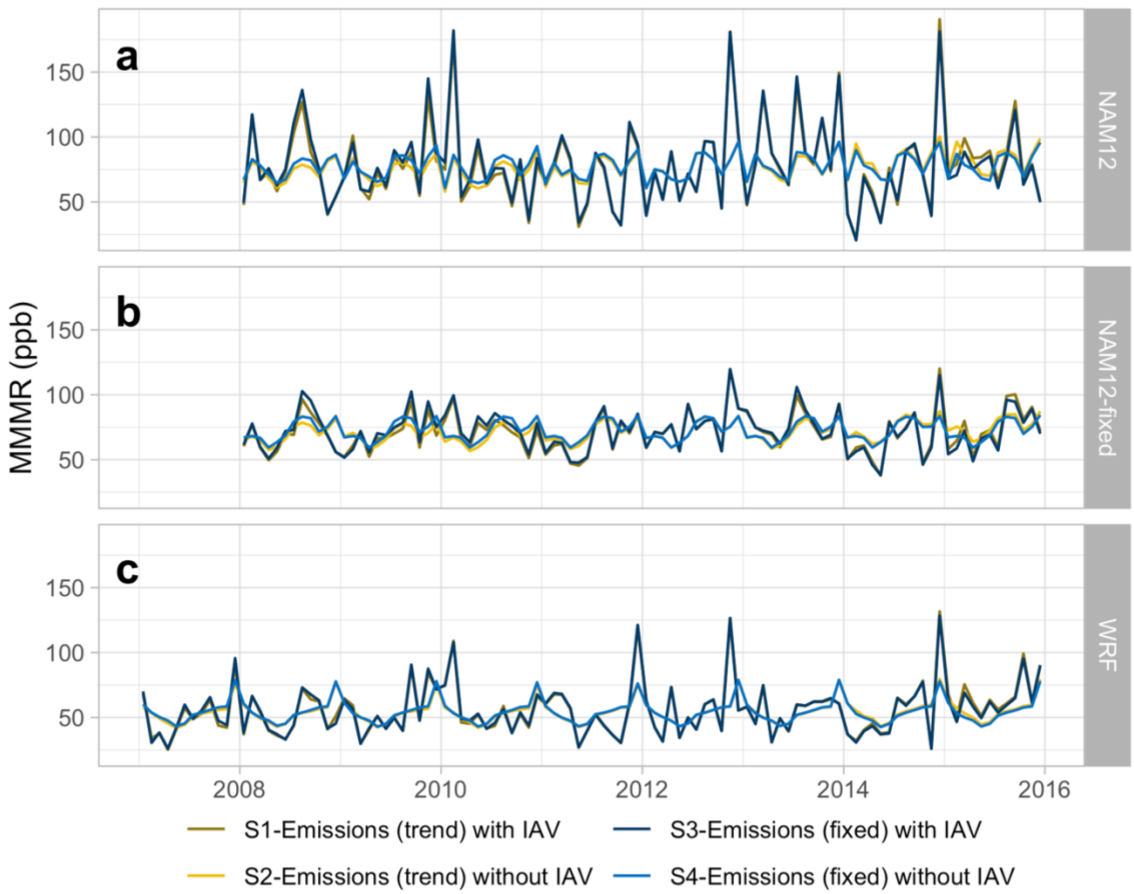

Figure S36. Comparison between monthly averaged MMR timeseries at site SGP for all 4 modeling scenarios using NAM12, NAM12 with fixed sampling time, and WRF meteorology products

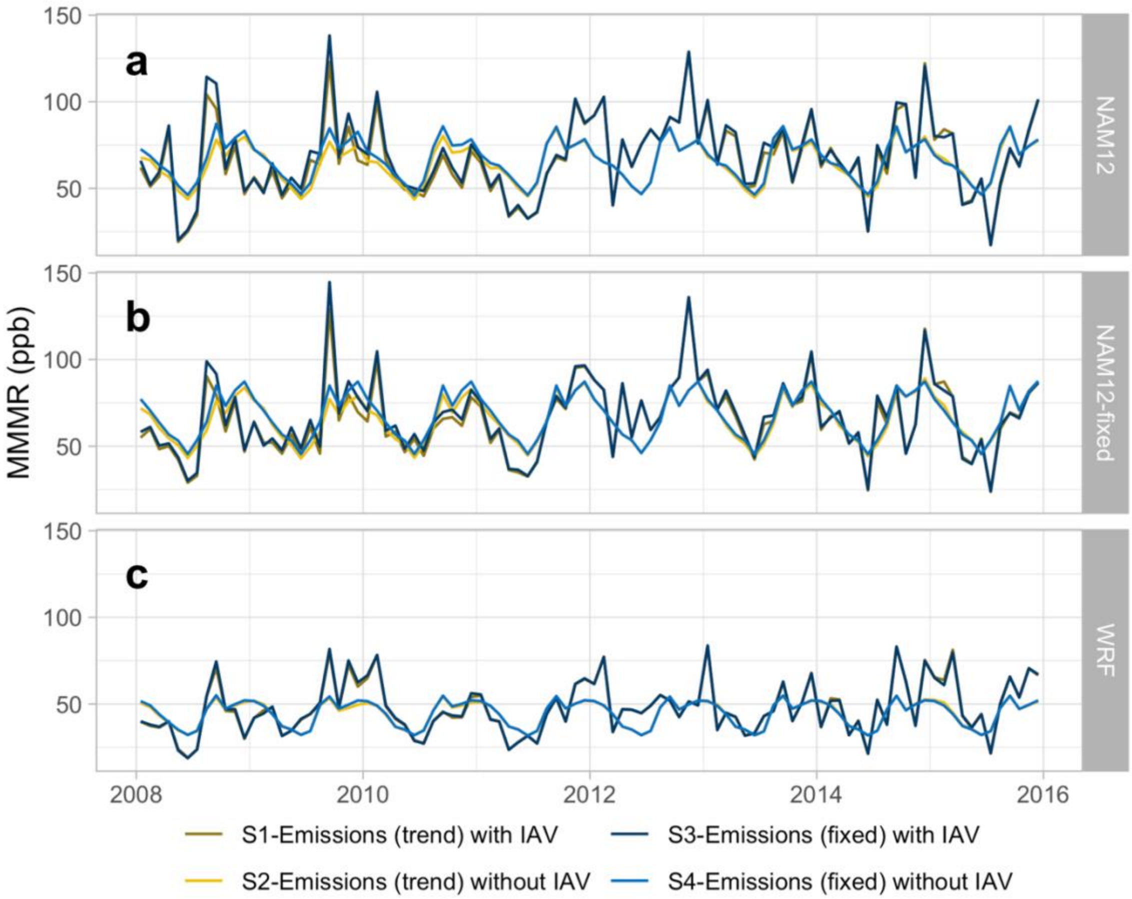

Figure S37. Comparison between monthly averaged MMR timeseries at site WKT for all 4 modeling scenarios using NAM12, NAM12 with fixed sampling time, and WRF meteorology products